AFATL-TR-89-49

AD-A213 379

An Autopilot Design Methodology for Bank-to-Turn Missiles

Roger L Smith, Captain, USAF

GUIDANCE & CONTROL BRANCH
AEROMECHANICS DIVISION

AUGUST 1989

INTERIM REPORT FOR PERIOD MARCH 1988 - APRIL 1989

AIR FORCE ARMAMENT LABORATORY
Air Force Systems Command ▮ United States Air Force ▮ Eglin Air Force Base, Florida

NOTICE

When Government drawings, specifications, or other data are used for any purpose other than in connection with a definitely related Government procurement operation, the United States Government thereby incurs no responsibility nor any obligation whatsoever; and the fact that the Government may have formulated, furnished, or in any way supplied the said drawings, specifications, or other data, is not to be regarded by implication or otherwise as in any manner licensing the holder or any other person or corporation, or conveying any rights or permission to manufacture, use, or sell any patented invention that may in any way be related thereto.

This report has been reviewed by the Public Affairs Office (PA) and is releasable to the National Technical Information Service (NTIS). At NTIS, it will be available to the general public, including foreign nations.

This technical report has been reviewed and is approved for publication.

FOR THE COMMANDER

Stephen C. Korn

STEPHEN C. KORN
Technical Director, Aeromechanics Division

If your address has changed, if you wish to be removed from our mailing list, or if the addressee is no longer employed by your organization, please notify AFATL/FXG , Eglin AFB FL 32542-5434.

Copies of this report should not be returned unless return is required by security considerations, contractual obligations, or notice on a specific document.

UNCLASSIFIED
SECURITY CLASSIFICATION OF THIS PAGE

REPORT DOCUMENTATION PAGE

Form Approved OMB No. 0704-0188

1a. REPORT SECURITY CLASSIFICATION Unclassified	1b. RESTRICTIVE MARKINGS
2a. SECURITY CLASSIFICATION AUTHORITY	3. DISTRIBUTION/AVAILABILITY OF REPORT Approved for public release; distribution is unlimited.
2b. DECLASSIFICATION/DOWNGRADING SCHEDULE	
4. PERFORMING ORGANIZATION REPORT NUMBER(S)	5. MONITORING ORGANIZATION REPORT NUMBER(S) AFATL-TR-89-49
6a. NAME OF PERFORMING ORGANIZATION Guidance and Control Branch Aeromechanics Division 6b. OFFICE SYMBOL (If applicable) AFATL/FXG	7a. NAME OF MONITORING ORGANIZATION
6c. ADDRESS (City, State, and ZIP Code) Air Force Armament Laboratory Eglin AFB FL 32542-5434	7b. ADDRESS (City, State, and ZIP Code)
8a. NAME OF FUNDING/SPONSORING ORGANIZATION Aeromechanics Division 8b. OFFICE SYMBOL (If applicable) AFATL/FX	9. PROCUREMENT INSTRUMENT IDENTIFICATION NUMBER
8c. ADDRESS (City, State, and ZIP Code) Air Force Armament Laboratory Eglin AFB FL 32542-5434	10. SOURCE OF FUNDING NUMBERS PROGRAM ELEMENT NO. 62602F PROJECT NO. 2567 TASK NO. 01 WORK UNIT ACCESSION NO. 25

11. TITLE (Include Security Classification)
An Autopilot Design Methodology for Bank-to-Turn Missiles

12. PERSONAL AUTHOR(S)
Capt Roger L. Smith

13a. TYPE OF REPORT	13b. TIME COVERED	14. DATE OF REPORT (Year, Month, Day)	15. PAGE COUNT
Interim	FROM Mar 88 TO Apr 89	August 1989	108

16. SUPPLEMENTARY NOTATION
Availability of report is specified on front cover.

17. COSATI CODES			18. SUBJECT TERMS (Continue on reverse if necessary and identify by block number)
FIELD	GROUP	SUB-GROUP	Bank-to-Turn, Modern Control, Gain Scheduling
0902	1707		

19. ABSTRACT (Continue on reverse if necessary and identify by block number)

Complete use of the multiinput/multioutput (MIMO) capability of modern control theory is utilized by employing a 3-axis, fully coupled autopilot design for the extended medium range air-to-air technology (EMRAAT) airframe. With the exception of the drag equation, all nonlinear dynamics (including coriolis and gyroscopic terms) are retained prior to model linearization. Discrete linear quadratic regulator theory is used for controller designs. Gain scheduling is addressed in a stochastic manner allowing large random parametric variations in missile roll, pitch, yaw rates, angle-of-attack, and sideslip. This is in contrast to most modern design methodologies which in spite of the MIMO capability of modern control separate one axis from the other two (either roll from yaw/pitch or pitch from yaw/roll) in a decoupled design strategy. It also contrasts the common practice in which many of the nonlinear terms are discarded prior to modelling. The 3-axis design provides a means of assessing roll, pitch, and yaw interactions; and, the benefits of this design philosophy are illustrated in a comparison with a traditional design using the same airframe.

20. DISTRIBUTION/AVAILABILITY OF ABSTRACT	21. ABSTRACT SECURITY CLASSIFICATION	
☐ UNCLASSIFIED/UNLIMITED ☒ SAME AS RPT. ☐ DTIC USERS	Unclassified	
22a. NAME OF RESPONSIBLE INDIVIDUAL ROGER L. SMITH, Capt, USAF	22b. TELEPHONE (Include Area Code) 882-2961	22c. OFFICE SYMBOL AFATL/FXG

DD Form 1473, JUN 86 *Previous editions are obsolete.* SECURITY CLASSIFICATION OF THIS PAGE

UNCLASSIFIED

PREFACE

This report documents results obtained in the In-House Autopilot program. The program was sponsored and performed by the Flight Controls Technology (FCT) Section, the Guidance and Control Branch (FXG), Air Force Armament Laboratory (AFATL), Eglin Air Force Base, Florida. The effort was performed during the period of March 1988 to April 1989.

This program is an in-house effort that was initiated in March 1988. The scheduled completion date for the program is September 1992. The short term objective of the program was to extend the autopilot design of the Advanced Robust Autopilot program, contract No. F08635-87-C-0163, to a roll/pitch/yaw autopilot and retain all nonlinear terms prior to model linearization. The long term objectives of the program are to develop an autopilot design strategy to reduce the level of ad-hoc engineering used in autopilot design and evaluate promising basic research in missile control theory for potential system applications.

Primary FCT personnel involved in the effort were Capt Kenneth Welzyn, program manager, Capt Roger L. Smith, Principal Investigator, Dr James R. Cloutier, Technical Advisor, and Mr Johnny Evers, Section Supervisor.

TABLE OF CONTENTS

TABLE OF CONTENTS (CONCLUDED)

LIST OF FIGURES

LIST OF TABLES

LIST OF SYMBOLS

This section lists the more commonly used symbols.

α	Angle-of-attack
α_I	$\int \alpha \, dt$
β	Sideslip angle
δ_p	Aileron
δ_q	Elevator
δ_r	Rudder
δ_1, δ_2, δ_3, δ_4	Missile control surfaces
ϕ, θ, ψ	Missile Euler angles
A, B	Continuous system matrices
a_{y_I}	Achieved acceleration along the inertial y-axis
a_{z_I}	Achieved acceleration along the inertial z-axis
C_{N_α}	Aerodynamic force derivative in the pitch plane due to α. Note that this is obtained by taking the slope of the aerodynamice derivative C_N.
$C_{N_{\dot{\alpha}}}$	Aerodynamic force derivative in the pitch plane due to $\dot{\alpha}$
C_{N_q}	Aerodynamic force derivative in the pitch plane due to q

$C_{N_{\delta q}}$ Aerodynamic force derivative in the pitch plane due δ_q

C_{Y_β} Aerodynamic force derivative in the yaw plane due to β

C_{Y_p} Aerodynamic force derivative in the yaw plane due to p

C_{Y_r} Aerodynamic force derivative in the yaw plane due to r

$C_{Y_{\delta p}}$ Aerodynamic force derivative in the yaw plane due to δ_p

$C_{Y_{\delta r}}$ Aerodynamic force derivative in the yaw plane due to δ_r

C_{l_β} Aerodynamic moment derivative in the roll plane due to β

C_{l_p} Aerodynamic moment derivative in the roll plane due to p

C_{l_r} Aerodynamic moment derivative in the roll plane due to r

$C_{l_{\delta p}}$ Aerodynamic moment derivative in the roll plane due to δ_p

$C_{l_{\delta r}}$ Aerodynamic moment derivative in the roll plane due to δ_r

C_{m_α} Aerodynamic moment derivative in the pitch plane due to α

$C_{m_{\dot{\alpha}}}$	Aerodynamic moment derivative in the pitch plane due to $\dot{\alpha}$
C_{m_q}	Aerodynamic moment derivative in the pitch plane due to q
$C_{m_{\delta q}}$	Aerodynamic moment derivative in the pitch plane due to δ_q
C_{n_β}	Aerodynamic moment derivative in the yaw plane due to β
C_{n_p}	Aerodynamic moment derivative in the yaw plane due to p
C_{n_r}	Aerodynamic moment derivative in the yaw plane due to r
$C_{n_{\delta p}}$	Aerodynamic moment derivative in the yaw plane due to δ_p
$C_{n_{\delta r}}$	Aerodynamic moment derivative in the yaw plane due to δ_r
d	Missile reference diameter
F_X, F_Y, F_Z	Missile force components
g	Gravity (also used to describe missile or target acceleration where the term (g's) refers to the ratio of acceleration to the acceleration of gravity)
J	Inertia matrix
k	Gain Matrix

Mach	Ratio of missile or target speed to the speed of sound at a given altitude
p	roll rate
p_I	$\int p \, dt$
q	pitch rate
Q	Dynamic Pressure
r	Yaw rate
S	Missile reference area
u,v,w	Missile velocity components
u	Control Vector: $\left[\delta_p \quad \delta_q \quad \delta_r\right]^T$
V	Total missile velocity
W	Missile weight
x	Continuous system state vector: $\left[\alpha \quad \beta \quad p \quad q \quad r\right]^T$
x_D	Discrete system state vector: $\left[\alpha \quad \beta \quad p \quad q \quad r \quad \alpha_I \quad p_I \quad \delta_p \quad \delta_q \quad \delta_r\right]^T$
x_I	Augmented continuous states: $\left[\alpha \quad \beta \quad p \quad q \quad r \quad \alpha_I \quad p_I\right]^T$

SECTION I

INTRODUCTION

1. OBJECTIVE

This report documents an autopilot design for a tactical bank-to-turn air-to-air missile that must intercept a highly maneuverable target. The approach used in this study takes into account the aerodynamic and inertial interactions (cross coupling effects) that are common to this type of problem. This approach is different from many approaches to air-to-air missile autopilot design since some effects of coupling (primarily inertial) are often neglected during the design stages of the autopilots. Such neglecting of terms leads to a simplified nonlinear model. The approach taken for the project is to develop the linearized model from a full nonlinear model. A stochastic approach is applied to gain scheduling which allows large random parametric variations, this approach leads to simplified gain scheduling requirements. It is expected that this approach will enhance the performance of the autopilot in the presence of sensor noise and modeling errors. Improved performance leads to decreased miss distances during the missile-target intercepts.

2. TERMINOLOGY AND REFERENCE FRAMES USED

Figure 1 shows the missile body coordinate frame which is used to describe the six-degrees-of-freedom (6 DOF) for a missile. Three-degrees-of-freedom are associated with the missile body position and the other three-degrees-of-freedom are associated with the missile body angular orientation.

The missile body center of mass is the origin for the coordinate frame. From Figure 1 it should be apparent that the x axis passes through the center of mass of the missile from the rear to the front. The y axis passes through the center of mass of the missile from the left side of the missile to the right side of the missile. The z axis

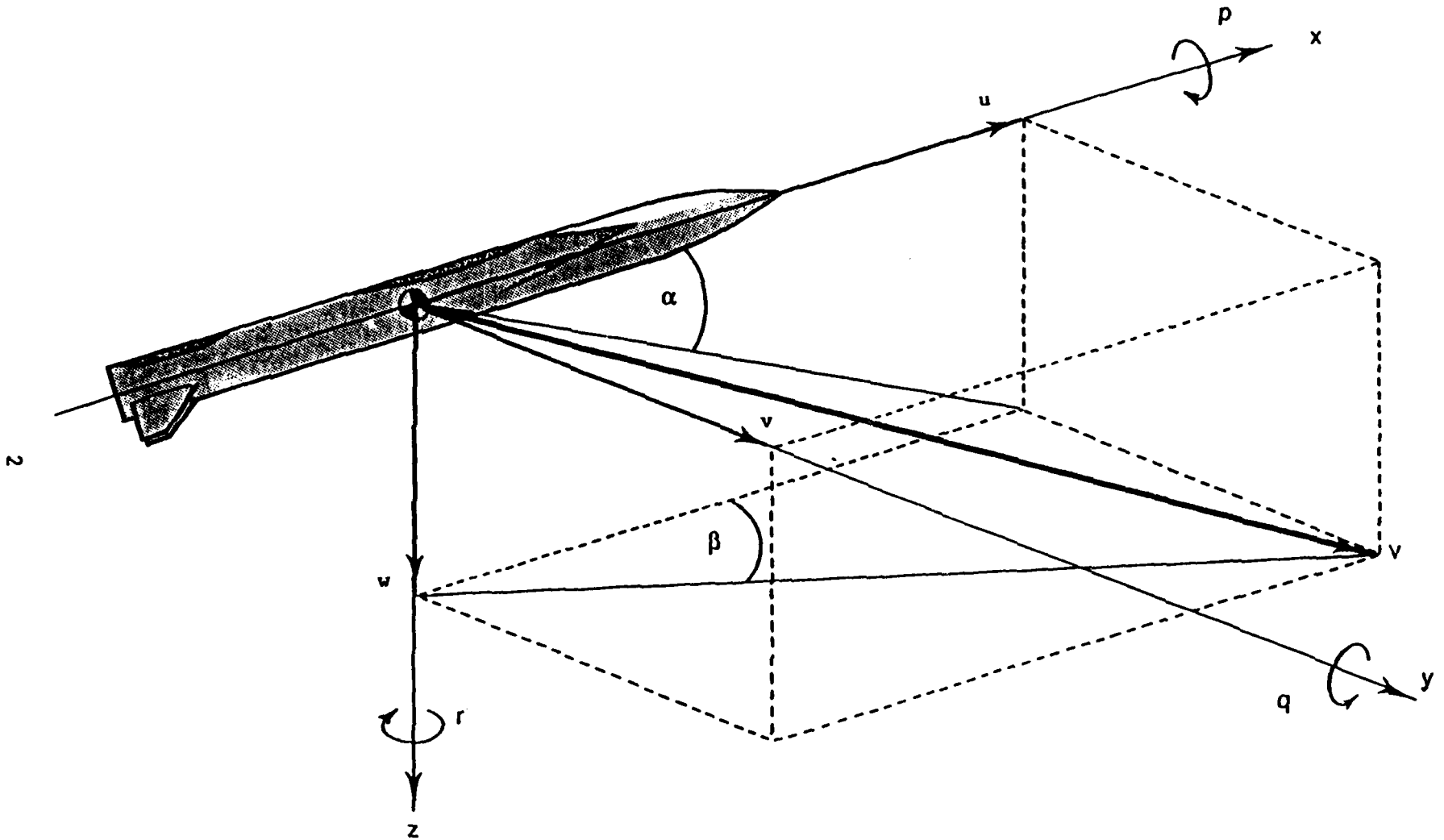

Figure 1. Missile Body Coordinate Frame

passes through the center of mass of the missile from the top of the missile to the bottom.

The missile body velocity components u, v, and w lie along the x, y, and z axis, correspondingly. The right hand rule defines the sense of the rotation about the three axes. The angular rotations about the x, y, and z axes are correspondingly called roll, pitch, and yaw angles. The term body rates is used to describe the rotation rates (roll, yaw, and pitch rates) about the x, y, and z axis.

Three planes can be defined from Figure 1. The y and z axis form the roll plane. The x and y axis form the yaw plane. The x and z axis form the pitch plane. The angle-of-attack (α) is the angle formed in the pitch plane between the missile longitudinal (x axis) and the z component of the total missile body velocity vector. The sideslip angle (β) is the angle formed in the yaw plane between the missile longitudinal axis and the y component of the total missile body velocity vector.

Figure 2 shows the inertial reference frame. Note, that the Z_I axis as shown is positive down. Shown in Figure 2 are azimuth and elevation angles, and the relative range (R) from the missile to the target. This figure is primarily used to describe the missile-target intercept. The inertial reference frame can be transformed into the missile body reference frame by using Euler angles. The Euler angles ϕ, θ, and ψ are used to describe the angles of rotation needed for the inertial reference frame to come into coincidence with the missile body reference frame. There is a specific order to the rotation. First, the inertial reference frame is rotated about the Z_I axis through the angle ψ. Second, the inertial reference frame is rotated about the new Y_I axis through the angle θ. Finally, the inertial reference frame is rotated about the new X_I axis.

3. THE BANK-TO-TURN CONTROL PROBLEM

In Reference 1, Arrow summarizes preferred orientation control for tactical missiles. Missile steering falls into two basic categories: skid-to-turn (STT) and bank-to-turn (BTT) control. STT control is prevalent in most existing guided weapons. In STT control the maneuvers

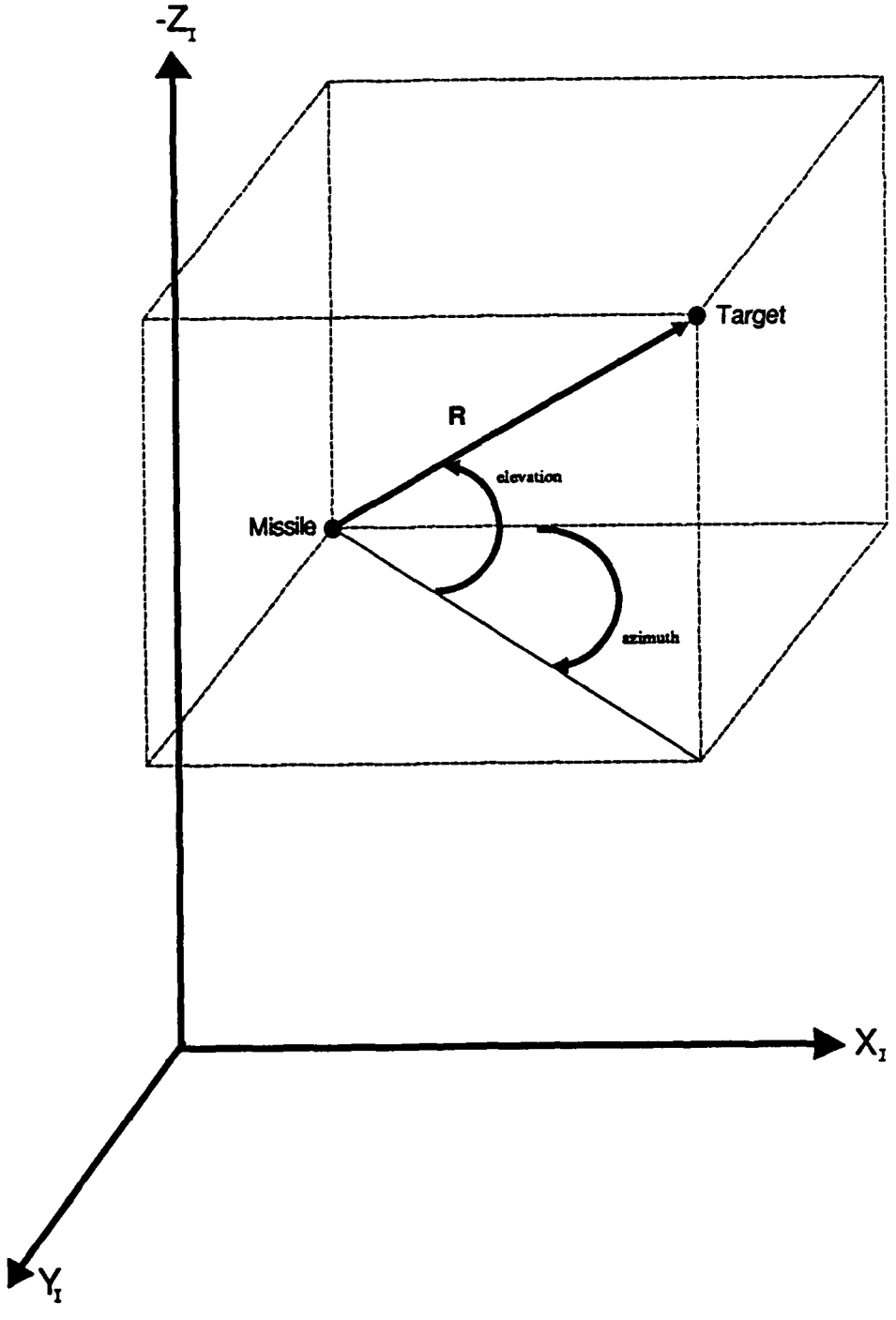

Figure 2. Inertial Reference Frame

are done in the pitch and yaw plane with the missile roll stabilized. In BTT control the maneuvers are primarily done in the roll and pitch planes while control may be used to minimize sideslip. BTT control of the missile is similar in nature to how pilots might fly their aircraft, Reference 2. BTT missiles have only recently begun to receive more attention for their possible use in air-to-air applications. BTT vehicles have two chief advantages over STT vehicles. The first is that BTT vehicles can travel farther with the same amount of fuel. BTT vehicles also have a much larger acceleration capability in the preferred maneuver plane than STT vehicles.

BTT steering may be placed into categories such as BTT 180, BTT 90, and coordinated BTT (CBTT). BTT 180 means the airframe may be commanded to roll as much as 180 degrees before acceleration. BTT 90 airframes may roll up to 90 degrees. CBTT implies the entire maneuver is coordinated so that the airframe is commanded to accelerate in a specified direction before the roll maneuver completes. The airframe used in this study is a BTT 180 airframe and uses CBTT command logic to command the autopilot.

BTT airframes are capable of high roll rates which induce undesirable yawing and pitching moments in the airframe. The asymmetrical properties of BTT airframes lead to a requirement to minimize sideslip since large sideslip angles have a negative affect on pitch and roll dynamics. Another requirement to minimize sideslip is to prevent the air intake for air breathing missiles from being reduced to the point that the propulsion unit fails (this is called flameout).

4. MISSILE CROSS COUPLING

BTT missiles are asymmetrical airframes, and the lack of symmetry leads to increased gyroscopic and inertial coupling of roll, pitch, and yaw rates. The roll rate coupling may be the most severe of the three. Since BTT control is used, the airframe must be capable of attaining high roll rates. These high roll rates are coupled into the pitch and yaw dynamics. When the assumption is made that the airframe is symmetrical some of the cross coupling terms are assumed to be negligible in the moment equations. This assumption is primarily

valid for STT airframes which usually are nearly symmetrical. This assumption also leads to a simplified nonlinear model. In the approach used for this problem, symmetry is not assumed; hence, the cross coupling terms are not immediately assumed to be negligible.

Aerodynamic cross coupling also affects the roll, pitch and yaw dynamics. The aerodynamic flying qualities and coupling effects are normally obtained through wind tunnel testing. The effects of aerodynamic coupling are then clearly a function of each of these coefficients and will vary from one airframe to the next.

5. AUTOPILOT

Figure 3 shows a simplified missile system block diagram. As shown in Figure 3, the autopilot consists of the BTT logic and a controller with a gain scheduler. Since the controller is based on a linearized model, gain scheduling is required to implement a piecewise linear controller. Gain scheduling consists of gain lookup tables that allow gains to change with varying parameters. The autopilot takes the guidance law commands, which are commanded accelerations in the body frame, and develops commands for the actuators. The actuators move the missile control surfaces (fins). The aileron, elevator, and rudder deflection commands are mixed to develop commands for the four actuators.

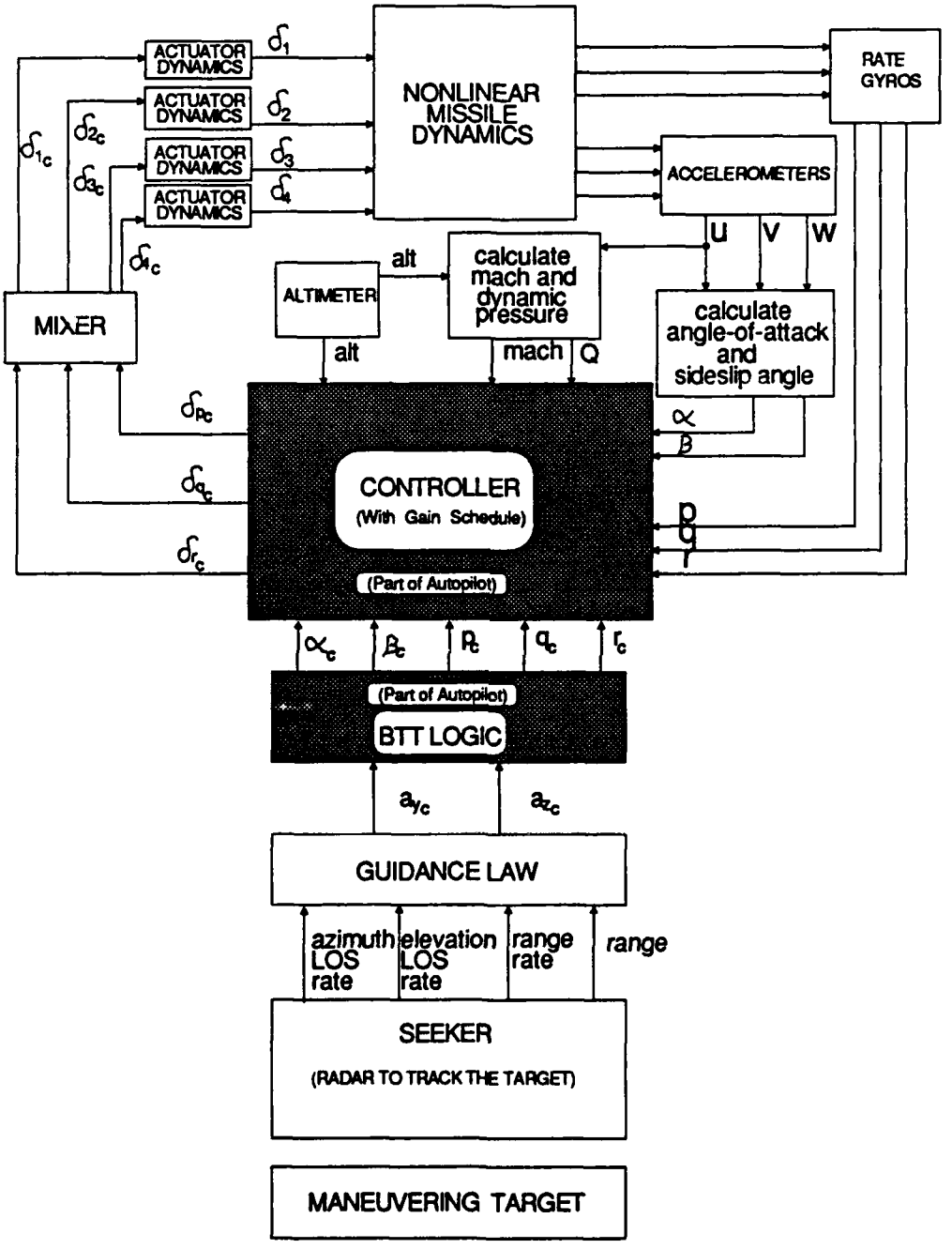

Figure 3. Missile System Block Diagram

SECTION II
PREVIOUS WORK

Many studies for BTT autopilots have been conducted during the past several years. Approaches to autopilot design range from classical designs to linear quadratic regulator (LQR), linear quadratic gaussian/loop transfer recovery (LQG/LTR), pole placement, and eigenstructure assignment designs. An assessment of BTT autopilot technology is provided by Cloutier, Evers, and Feely in Reference 3.

1. CLASSICAL DESIGNS

In one approach roll, pitch, and yaw autopilots were independently designed and the roll command from the roll autopilot fed to the pitch and yaw autopilots, Reference 4. The intent was to coordinate the roll and yaw motion and minimize coupling of roll and yaw dynamics into the pitch dynamics. In this approach the yaw command follows the roll command; this minimizes sideslip and is termed as a coordinated bank-to-turn steering.

In another design, a dither adaptive approach was used to independently design roll, pitch and yaw autopilots, Reference 5. In this approach a dither signal is injected and the adaptive network is used to tune the rate and acceleration loop gains of the autopilots.

2. MODERN DESIGNS

An LQG/LTR pitch/yaw autopilot based on a model with the roll dynamics decoupled from the pitch/yaw dynamics was designed with pole placement techniques used for the roll autopilot, Reference 6. Gyroscopic coupling of the roll dynamics into the pitch dynamics was included by developing linear pitch/yaw models at fixed, nonzero roll rates. The autopilot gains were scheduled as a function of roll rate and dynamic pressure.

In another variation, an LQR design with the pitch dynamics decoupled from the roll/yaw dynamics was designed, Reference 7. Both the pitch and roll/yaw autopilots were developed with LQR techniques. Pitch dynamics entered the roll/yaw design since the roll/yaw model was

linearized about fixed angles-of-attack. The design was digital and included a computational delay. The resulting controller was scheduled as a function of angle-of-attack. Dynamic pressure was excluded from the schedule since performance comparisons were done at fixed altitudes. Much of this work is used as a basis for this thesis.

In a comparison of a modern control approach to a classical approach Arrow and Williams state that classical approaches can fall short of modern approaches in ease of finding a control law for a highly coupled system, Reference 8. They also state the classical approach deals better with unmodeled constraints.

In Reference 9, Nesline and Zarchan demonstrate the benefits of analyzing modern control designs using classical frequency response techniques. The purpose is to identify unmodeled disturbances that potentially may destabilize the modern design.

3. DECOUPLED MISSILE DYNAMICS

The thrust of these studies still centers around decoupled designs. In these decoupled approaches the nonlinear model is simplified before the linear model is developed. In most approaches to simplifying the nonlinear model the basic assumption is that the effects of dropping the inertial cross coupling terms are minimal. In most cases this may in fact be true since aerodynamic forces and moments tend to dominate the missile dynamics. The validity of the assumption is tested by evaluating the performance of the autopilot in a detailed nonlinear missile simulation which includes all dynamics.

Multiple input, multiple output designs are available with modern control approaches, which leads one to expect autopilot designs based on the full roll/pitch/yaw missile dynamics (roll/pitch/yaw autopilots) should be more prevalent when modern control approaches are used. One reason for the lack of roll/pitch/yaw designs may be the influence of past classical autopilot design approaches. Previously, most air-to-air missiles were STT and with symmetrical qualities. This simplified the design considerations, and allowed treatment of the problem with classical designs for single input single output systems. Also, depending on the airframe, a decoupled autopilot design may be desirable

since the decision to decouple the design is based on some insight into the airframe characteristics. Based on the linear model for the airframe used in this study it still appears that a roll/pitch/yaw design based on the full nonlinear model should lead to increased robustness and at the very least offer a means of evaluating the decoupled approaches.

SECTION III

NONLINEAR AIRFRAME

1. DESCRIPTION

The extended medium range air-to-air technology (EMRAAT) airframe is used in this study. The EMRAAT is a BTT airframe with four control surfaces (fins) that are controlled by actuators. Figure 4 shows a diagram of the airframe used. As can be seen in this figure the airframe is asymmetric. The top of the airframe is flat and the tail fins are not cruciform. Cruciform fins form four 90 degree angles unlike the fins shown in Figure 4. This airframe has one preferred maneuver plane which is normal to the bottom surface of the missile. This implies the airframe may have to roll as much as 180 degrees to achieve a particular maneuver.

2. EULER EQUATIONS OF MOTION

Missiles, as with any airframes, have six degrees of freedom which are described by the Euler equations of aerodynamic motion. The Euler equations describe the forces and moments acting on the missile. The six degrees of freedom are based on a missile body coordinate frame as shown in Figure 5. Three equations describe the forces acting on the missile body. The three force equations are as follows:

$$F_X + T_X + W_X = \frac{W}{g}\left(\dot{u} + qw - rv\right) \tag{1}$$

$$F_Y + T_Y + W_Y = \frac{W}{g}\left(\dot{v} + ru - pw\right) \tag{2}$$

$$F_Z + T_Z + W_Z = \frac{W}{g}\left(\dot{w} - qu + pv\right) \tag{3}$$

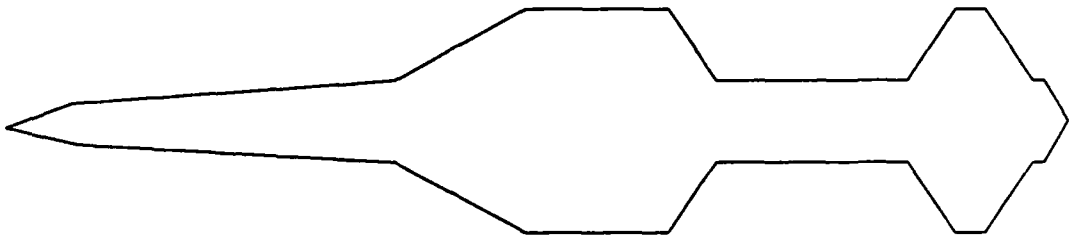

Top View

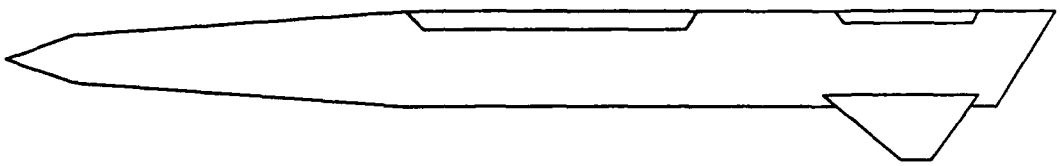

Side View

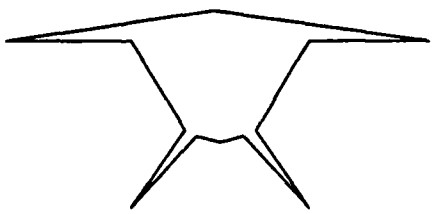

Rear View

Figure 4. EMRAAT Airframe

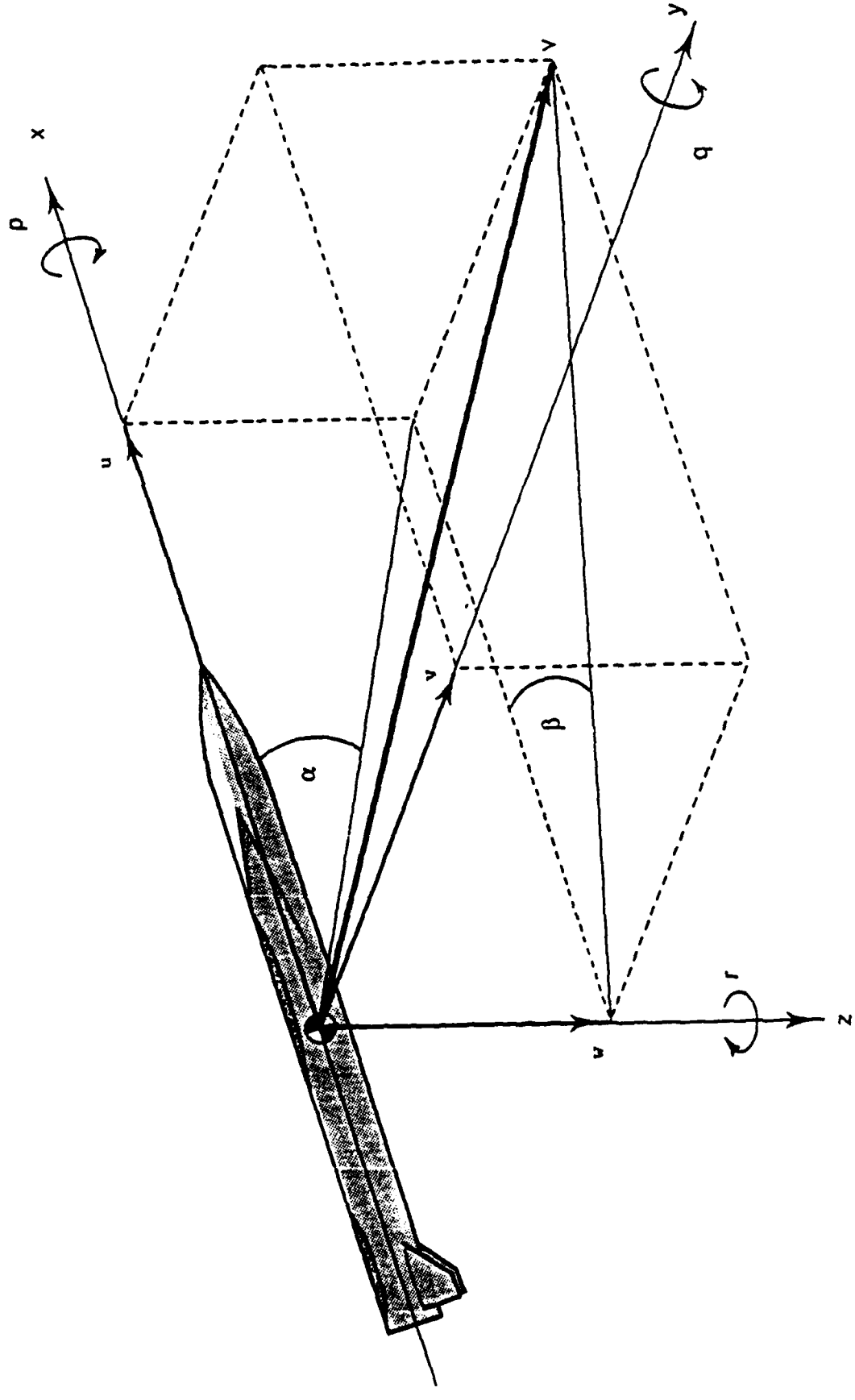

Figure 5. Missile Body Coordinate Frame

In Equations (1), (2), and (3), u, v, and w denote the missile body velocities. The variables p, q, and r denote the respective roll, pitch and yaw rates. F_X, F_Y, and F_Z are force components that are defined by data for each specific airframe. Wind tunnel testing is used to obtain this data. T_X, T_Y, and T_Z are forces as a result of the thrust components acting on the missile. This information is based on the motor used for the airframe. W_X, W_Y, and W_Z are the forces acting on the missile due to the missile weight components. W is the missile weight and g is gravity.

Three equations describe the moments acting on the missile. These three moment equations are as follows

$$l = I_{XX}\dot{p} - \left(I_{YY} - I_{ZZ}\right)qr + I_{YZ}\left(r^2 - q^2\right) - I_{XX}\left(pq + \dot{r}\right) + I_{XY}\left(rp - \dot{q}\right) \tag{4}$$

$$m = I_{YY}\dot{q} - \left(I_{ZZ} - I_{XX}\right)rp + I_{XZ}\left(p^2 - r^2\right) - I_{XY}\left(qr + \dot{p}\right) + I_{YZ}\left(pq - \dot{r}\right) \tag{5}$$

$$n = I_{ZZ}\dot{r} - \left(I_{XX} - I_{YY}\right)pq + I_{XY}\left(q^2 - p^2\right) - I_{YZ}\left(rp + \dot{q}\right) + I_{XZ}\left(qr - \dot{p}\right) \tag{6}$$

Where the moments of inertia are given by I_{XX}, I_{YY}, and I_{ZZ}. The products of inertia are given by I_{XY}, I_{XZ}, and I_{YZ}. Equations (4), (5) and (6) can be written in matrix form

$$\begin{bmatrix} l \\ m \\ n \end{bmatrix} = J^{-1} \begin{bmatrix} \dot{p} \\ \dot{q} \\ \dot{r} \end{bmatrix} + H(p,q,r) \tag{7}$$

Where

$$J = \begin{bmatrix} I_{XX} & -I_{XY} & -I_{XZ} \\ -I_{XY} & I_{YY} & -I_{YZ} \\ -I_{XZ} & -I_{YZ} & I_{ZZ} \end{bmatrix} \tag{8}$$

$$H = \begin{bmatrix} -(I_{YY} - I_{ZZ})qr + I_{YZ}(r^2 - q^2) - I_{XZ}pq + I_{XY}rp \\ -(I_{ZZ} - I_{XX})rp + I_{XZ}(p^2 - r^2) - I_{XY}qr + I_{YZ}pq \\ -(I_{XX} - I_{YY})pq + I_{XY}(q^2 - p^2) - I_{YZ}rp + I_{XZ}qr \end{bmatrix} \tag{9}$$

3. NONLINEAR AIRFRAME STATE EQUATIONS

This section presents the development of the nonlinear airframe model as used in this study and is based on the aerodynamic data for the airframe. This development leads to the five nonlinear state equations which are later linearized to get the linear model for the autopilot design. The force equations are developed first and then the moment equations are developed.

As was done in Reference 7, and other autopilot designs, Equation (1) is not included as part of the nonlinear airframe state equations. Equation (1) is included in the nonlinear six-degree-of-freedom missile simulation. For this study thrust is assumed to be zero, so

$$T_x = T_y = T_z = 0 \tag{10}$$

The force components for weight are given as

$$W_y = W\cos(\theta)\sin(\phi) \tag{11}$$

$$W_z = W\cos(\theta)\cos(\phi) \tag{12}$$

Where θ and ϕ are two of the three Euler angles that describe the inertial orientation of the missile body with respect to the body reference frame (Figure 5). Substituting Equations (11) and (12) into Equations (2) and (3) and solving for F_y and F_z yields

$$F_Y = \frac{W}{g}(\dot{v} + ru - pw) - W\cos(\theta)\sin(\phi) \tag{13}$$

$$F_Z = \frac{W}{g}(\dot{w} - qu + pv) - W\cos(\theta)\cos(\phi) \tag{14}$$

The angle-of attack and sideslip angle are given by

$$\alpha = \tan^{-1}\left(\frac{w}{u}\right) \tag{15}$$

$$\beta = \tan^{-1}\left(\frac{v}{u}\right) \tag{16}$$

During flight α and β will be small, so the following small angle approximations can be used:

$$\alpha \approx \frac{w}{u} \tag{17}$$

$$\beta \approx \frac{v}{u} \tag{18}$$

The total missile velocity (V) is given by

$$V = \left[(u^2 + v^2 + w^2)\right]^{1/2} \tag{19}$$

Since the missile speed is nearly constant and the largest component of the velocity is along the missile's x axis the following approximations can be used

$$u \approx V \tag{20}$$

$$\dot{u} \approx 0 \tag{21}$$

It follows from Equations (17) and (18) that

$$\dot{\alpha} \approx \frac{\dot{w}}{V} \tag{22}$$

$$\dot{\beta} \approx \frac{\dot{v}}{V} \tag{23}$$

Using these approximations, Equations (13) and (14) can be rewritten to eliminate u, v, and w, and introduce α, β, and V, as follows:

$$F_y = \frac{WV}{g}(\dot{\beta} + r - p\alpha) - W\cos(\theta)\sin(\phi) \tag{24}$$

$$F_z = \frac{WV}{g}(\dot{\alpha} - q + p\beta) - W\cos(\theta)\cos(\phi) \tag{25}$$

The Appendix lists the aerodynamic data for the EMRAAT airframe for two flight conditions, the first condition is 40,000 feet at mach 2.5, and the second condition is at 65,000 feet, at mach 3.0. The Appendix provides the aerodynamic force derivatives which are used to specify the left hand sides of Equations (24) and (25). Equations (24) and (25) can be written as (Reference 10)

$$F_y = (QS)\left[C_{Y_\beta}\beta + C_{Y_p}p + C_{Y_r}r + C_{Y_{\delta p}}\delta_p + C_{Y_{\delta r}}\delta_r\right] \tag{26}$$

$$F_Z = (QS)\left[C_{N_\alpha}\alpha + C_{N_{\dot\alpha}}\dot\alpha + C_{N_q}q + C_{N_{\delta q}}\delta_q\right] \tag{27}$$

Substituting Equation (26) and (27) into Equations (24) and (25) and solving for $\dot\alpha$ and $\dot\beta$ leads to

$$\dot\alpha = \left[1 - \frac{gQSC_{N_{\dot\alpha}}}{WV}\right]^{-1}\left[(q - p\beta) + \frac{gQS}{WV}\left[C_{N_\alpha}\alpha + C_{N_q}q + C_{N_{\delta q}}\delta_q\right] + \frac{g}{V}\cos(\theta)\sin(\phi)\right] \tag{28}$$

$$\dot{\beta} = \left[p\alpha - r + \frac{gQS}{WV} \left(C_{Y_\beta} \beta + C_{Y_p} p + C_{Y_r} r + C_{Y_{\delta p}} \delta_p \right. \right. \tag{29}$$

$$\left. \left. + C_{Y_{\delta r}} \delta_r \right) + \frac{g}{V} \cos(\theta)\cos(\phi) \right]$$

The state Equations (28) and (29) are the two force equations used in development of the linear model. The next step is the development of the state equations for the moments. Equation (7) can be solved to yield

$$\begin{bmatrix} \dot{p} \\ \dot{q} \\ \dot{r} \end{bmatrix} = J^{-1} \begin{bmatrix} l \\ m \\ n \end{bmatrix} - J^{-1} H(p,q,r) \tag{30}$$

Where H(p,q,r) is given by Equation (9). To complete Equation (30), the aerodynamic moments l, m, and n are provided as part of the data from the aerodynamic tables supplied in the appendix and can be written in the form (Reference 10)

$$l = QSd\left(C_{l_\beta} \beta + C_{l_p} p + C_{l_r} r + C_{l_{\delta p}} \delta_p + C_{l_{\delta r}} \delta r \right) \tag{31}$$

$$m = QSd\left(C_{m_\alpha} \alpha + C_{m_{\dot{\alpha}}} \dot{\alpha} + C_{m_q} q + C_{m_{\delta q}} \delta_q \right) \tag{32}$$

$$n = QSd\left(C_{n_\beta} \beta + C_{n_p} p + C_{n_r} r + C_{n_{\delta p}} \delta_p + C_{n_{\delta r}} \delta r \right) \tag{33}$$

The nonlinear model development is now complete. The five state nonlinear model from which the linearized model is developed is described by Equations (28), (29), and (30). The Appendix lists the values for the variables used in the equations. The states used in the model are

$$\mathbf{x} = \begin{bmatrix} \alpha & \beta & p & q & r \end{bmatrix}^T \tag{34}$$

4. MODEL SIMPLIFICATIONS NOT USED

A closer look at Equations (28) through (33) reveals the aerodynamic and inertial cross coupling present in a nonlinear airframe. The model as it was presented is the model that will be used for the autopilot design. It should be noted that in other approaches the model dynamics were simplified which leads to reduced order linearized models. Some assumptions that can be used to reduce the order of the model so the dynamics can be separated into a pitch model and a roll/yaw model are presented here.

In terms of the aerodynamic data provided for the EMRAAT airframe, Equations (26), (27), (31), (32), and (33) have no terms that couple the pitch dynamics to the yaw or roll dynamics. These equations do indicate there is aerodynamic coupling between the yaw and roll dynamics. This partially supports using two simplified models, one for the pitch dynamics and another for the roll/yaw dynamics.

The force equations are simplified first. Equation (28) shows some cross coupling of roll and yaw dynamics into the pitch dynamics. Equation (29) shows cross coupling of pitch and roll dynamics into the yaw dynamics. To remove the roll/yaw dynamics from Equation (28) the term $p\beta$ can be assumed to be negligible since β is assumed to be near zero. To remove the pitch dynamics from Equation (29) the term $p\alpha$ can be changed to $p\alpha_K$ where α_K is a constant based on the assumption that α is slowly changing.

The moment equations are now simplified. Based on the assumption that the airframe is nearly symmetrical, the moments of inertia I_{YY} and I_{ZZ} are treated as being equal and the products of inertia I_{XY}, I_{XZ}, and I_{YZ} are neglected. This assumption reduces the inertia matrix J in Equation (8) to

$$J = \begin{bmatrix} I_{XX} & 0 & 0 \\ 0 & I_{YY} & 0 \\ 0 & 0 & I_{ZZ} \end{bmatrix} \tag{35}$$

Equation (9) may also be reduced to

$$H = \begin{bmatrix} 0 \\ -(I_{ZZ}-I_{XX})rp \\ -(I_{XX}-I_{YY})pq \end{bmatrix} \tag{36}$$

Equation (30) when used with Equations (35) and (36) can now be separated into a model for the pitch dynamics and a model for the roll/yaw dynamics. This is one possible approach to simplifying the model. Other approaches have separated the model into roll dynamics and pitch/yaw dynamics. Classical approaches have separated the model into roll, pitch, and yaw models and later added feedback paths between controllers to account for cross-coupling.

5. MISSILE CONTROL SURFACES

Control for the missile accelerations along the y and z axis and the missile body accelerations is provided by the missile control surfaces. The control surfaces are shown in Figure 6. As can be seen in Figure 6 the tail configuration is not symmetrical. Clearly, controls will also interact to compound the overall problem of coupling. Equation (37) is the mixing logic required to transform the four control surfaces shown in Figure 6 to the aileron, elevator and rudder controls (δ_p, δ_q, and δ_r). Although not actual control surfaces, δ_p, δ_q, and δ_r are used in the aerodynamic data provided the EMRAAT airframe. Another reason δ_p, δ_q, and δ_r are used is that both aerodynamicists and flight controls engineers find it easier to think of the control surfaces in terms of aileron, elevator, and rudder.

$$\begin{bmatrix} \delta_p \\ \delta_q \\ \delta_r \end{bmatrix} = \begin{bmatrix} 0 & -1/2 & -1/2 & 0 \\ 0 & +1/2 & -1/2 & 0 \\ -1 & 0 & 0 & +1 \end{bmatrix} \begin{bmatrix} \delta_1 \\ \delta_2 \\ \delta_3 \\ \delta_4 \end{bmatrix} \tag{37}$$

6. SIX-DEGREE-OF-FREEDOM (6-DOF) MISSILE SIMULATION

The 6-DOF simulation embodies the full nonlinear dynamics for a guided missile system. Figure 7 shows a simplified subsystems model for a guided missile. These subsystems are implemented in the 6-DOF simulation with considerably more detail than can be shown on this diagram. The bold lines on the diagram indicate signal flow. The dashed lines indicate measurements.

The missile guidance consists of the seeker and a guidance law. The seeker modeled is an active seeker which means it is emitting energy to scan the target. Gimbal dynamics are not included in the seeker model. The information provided by the seeker to the guidance law

consists of the missile-target line-of-sight (LOS) angles, LOS angle rates, range, and range rate. The guidance law is proportional navigation and provides lateral acceleration commands to the BTT logic.

The inertial measurement unit (IMU) consists of accelerometers and rate-gyros to measure the missile body accelerations and missile body roll, pitch, and yaw rates (turning rates). Prefilters are used to filter the measurements. The parameters are used throughout the simulation.

The BTT logic uses the lateral acceleration commands from the guidance law and the IMU measurements to form the autopilot commands. Included in the BTT logic is an estimator to estimate α and β in the presence of wind and sensor noise.

The autopilot is implemented in the simulation as a discrete controller with a computational delay included. The autopilot gains are scheduled to develop a piece wise linear autopilot.

The actuators receive their commands from the autopilot to control the total airframe response. In the simulation, each actuator is modeled as a fifth order electromechanical model and includes rate limiting. The actuators move the missile control surfaces. The autopilot commands to the actuator are delayed by 6 ms to simulate a computational delay.

In Figure 7, the block containing the airframe dynamics includes the full nonlinear missile dynamics for the EMRAAT airframe. This block generates the airframe response to the actuator inputs.

Also included in the simulation is a maneuvering target capable of performing 9g maneuvers to evade the missile. The simulation calculates the time left for intercept to occur and if this time reaches a specified minimum threshold the target performs an evasive maneuver.

Two feedback loops should be apparent in Figure 7. The inner loop consists of the autopilot, BTT logic, actuators, airframe dynamics and the IMU. The outer loop includes the guidance and the inner loop.

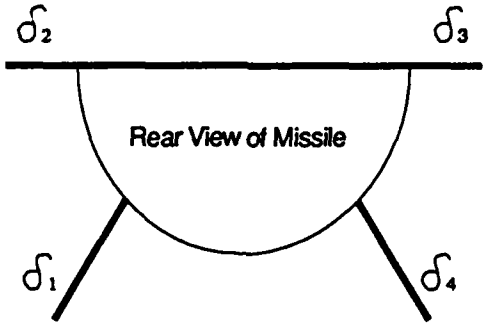

Figure 6. Control Surfaces

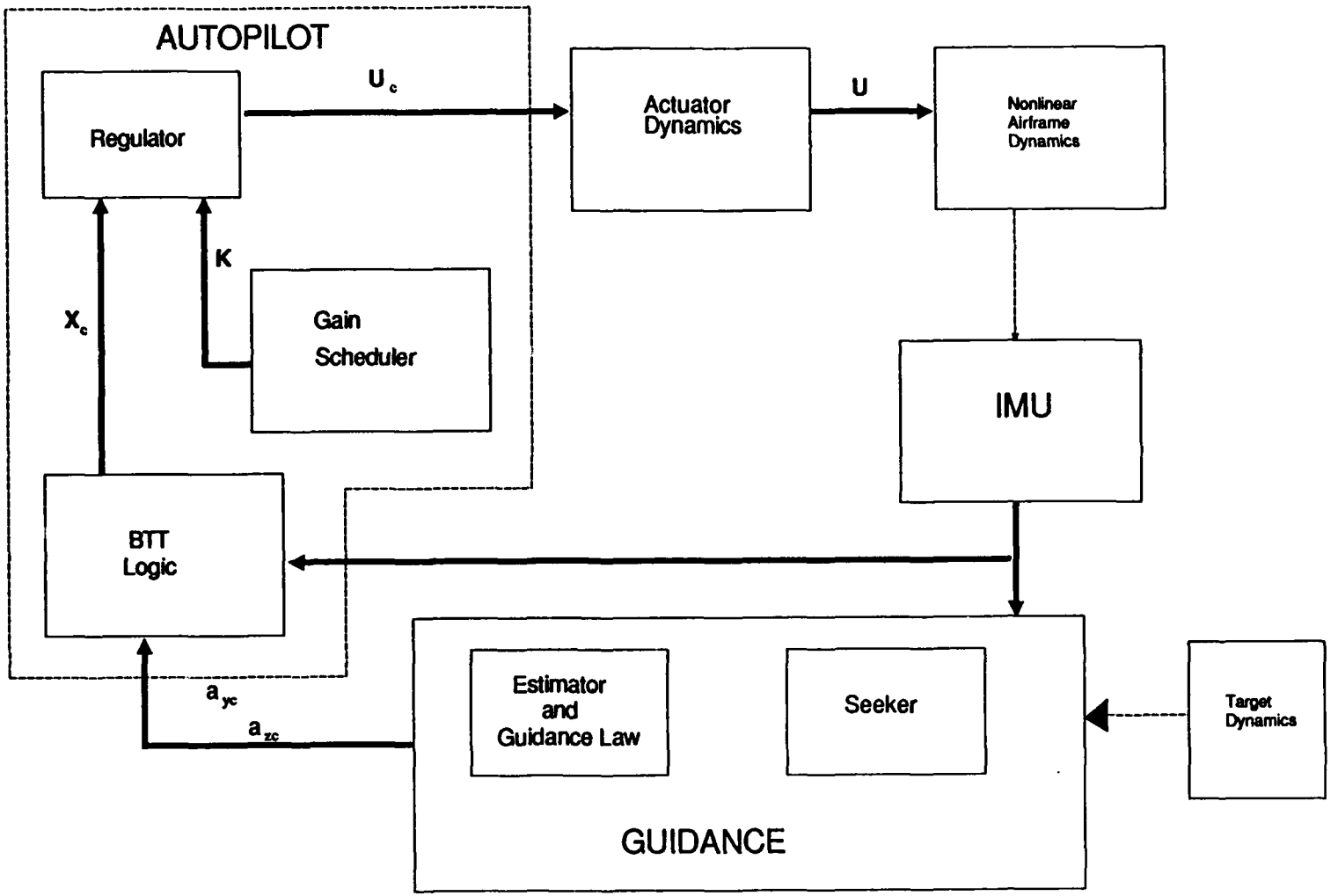

Figure 7. Guided Missile Subsystems

SECTION IV
LINEAR MODEL DEVELOPMENT

1. DEVELOPMENT OF THE LINEAR MODEL

The five state nonlinear model of Section III is now used to develop the linearized model. The nonlinear system

$$\dot{\mathbf{x}}(t) = \mathbf{f}(\mathbf{x}(t),\mathbf{u}(t)) \tag{38}$$

is linearized by using Reference 11 and leads to the linearized model

$$\dot{\mathbf{x}}(t) = \mathbf{A}\mathbf{x}(t) + \mathbf{B}\mathbf{u}(t) \tag{39}$$

Where **A** is given by

$$\mathbf{A} = \left.\frac{df}{dx}\right|_{\mathbf{x}_{nominal}} \tag{40}$$

and **B** is given by

$$\mathbf{B} = \left.\frac{df}{du}\right|_{\mathbf{x}_{nominal}} \tag{41}$$

and where $\Delta\mathbf{x}(t)$ and $\Delta\mathbf{u}(t)$ have been redefined to be $\mathbf{x}(t)$ and $\mathbf{u}(t)$ The system state and control vectors are

$$\mathbf{x}(t) = \begin{bmatrix}\alpha & \beta & p & q & r\end{bmatrix}^T \tag{42}$$

and

$$\mathbf{u}(t) = \begin{bmatrix}\delta_p & \delta_q & \delta_r\end{bmatrix}^T \tag{43}$$

Using Equations (40) and (41), the model is now ready to be linearized to yield the necessary equations for each element of the linear **A** and **B** system matrices. To simplify the equations let

$$\tilde{Q} = \frac{gQS}{VW} \tag{44}$$

and

$$Z_d = \left[1 - \frac{gQSC_{N_{\dot{\alpha}}}}{WV} \right] \tag{45}$$

Equations (28) and (29) are first linearized to yield the first two rows of **A** and **B**. The first element of **A** is found by taking the partial derivative of (28) with respect to α and leads to

$$a_{11} = \frac{C_{N_\alpha} \tilde{Q}}{Z_d} \tag{46}$$

Taking the partial derivative of Equation (28) with respect to β leads to

$$a_{12} = \frac{-p}{Z_d} \tag{47}$$

Taking the partial derivative of Equation (28) with respect to p leads to

$$a_{13} = \frac{-\beta}{Z_d} \tag{48}$$

Taking the partial derivative of Equation (28) with respect to q leads to

$$a_{14} = \frac{(1 + C_{N_q} \tilde{Q})}{Z_d} \tag{49}$$

Taking the partial derivative of Equation (28) with respect to r leads to

$$a_{15} = 0 \tag{50}$$

The first element in B is found by taking the partial derivative of (28) with respect to δ_p and leads to

$$b_{11} = 0 \tag{51}$$

The partial derivative of Equation (28) with respect to δ_q leads to

$$b_{12} = \frac{\tilde{Q}C_{N_{\delta q}}}{Z_d} \tag{52}$$

and the partial derivative of Equation (28) with respect to δ_r leads to

$$b_{13} = 0 \tag{53}$$

To find the second row elements for A and B, the procedure to find the row one elements is repeated with the exception that Equation (28) is now replaced with Equation (29) and the partial derivatives are taken with respect to q. The row 2 elements for A and B are found to be

$$a_{21} = p \tag{54}$$

$$a_{22} = \bar{Q}C_{Y_\beta} \tag{55}$$

$$a_{23} = \alpha + \bar{Q}C_{Y_p} \tag{56}$$

$$a_{24} = 0 \tag{57}$$

$$a_{25} = \bar{Q}C_{Y_p} \tag{58}$$

$$b_{21} = \bar{Q}C_{Y_{\delta p}} \tag{59}$$

$$b_{22} = 0 \tag{60}$$

$$b_{23} = \bar{Q}C_{Y_{\delta r}} \tag{61}$$

Extra steps are necessary to linearize the moment equations which will lead to rows 3, 4 and 5 for A and B. The first step is to multiply Equation (30) by the inertia matrix J and then linearize the right hand side of the result. This can be done since J is independent of the states. J will be included later in the linear model development. This leads to

$$J\begin{bmatrix} \dot{p} \\ \dot{q} \\ \dot{r} \end{bmatrix} = \begin{bmatrix} l \\ m \\ n \end{bmatrix} - H \tag{62}$$

Linearization of Equation (62) leads to the matrices M and N which will become part of matrices A and B. The matrix M is given by

$$M = \left.\frac{d\left[l\ m\ n\right]^T}{dx}\right|_{x_{nominal}} - \left.\frac{dH}{dx}\right|_{x_{nominal}} \tag{63}$$

and the matrix N is given by

$$N = \left.\frac{d\left[l\ m\ n\right]^T}{du}\right|_{x_{nominal}} - \left.\frac{dH}{du}\right|_{x_{nominal}} \tag{64}$$

The matrix H is given by (9), and l, m, and n are given by Equations (31), (32), and (33). The first row of M and N is found by taking the partial derivative of the first row in Equation (62) with respect to the elements in **x** and **u**. This leads to

$$m_{11} = 0 \tag{65}$$

$$m_{12} = QSdC_{l_\beta} \tag{66}$$

$$m_{13} = I_{XZ}q - I_{XY}r + QSdC_{l_p} \tag{67}$$

$$m_{14} = (I_{YY}-I_{ZZ})r + 2qI_{YZ} + pI_{XZ} \tag{68}$$

$$m_{15} = (I_{YY}-I_{ZZ})q - 2rI_{YZ} - I_{XY}p + QSdC_{l_r} \tag{69}$$

$$n_{11} = QSdC_{l_{\delta p}} \tag{70}$$

$$n_{12} = 0 \tag{71}$$

$$n_{13} = QSdC_{l_{\delta r}} \tag{72}$$

For m_{21} to m_{25}, and n_{21} to n_{23} the $\dot{\alpha}$ derivatives must be included. Taking the partial derivatives of row 2 of Equation (62) with respect to each of the elements in $\mathbf{x}$ and $\mathbf{u}$ leads to

$$m_{21} = QSd\left[C_{M_\alpha} + \frac{Q\tilde{C}_{M_{\dot{\alpha}}}}{Z_d}\right] \tag{73}$$

$$m_{22} = QSdC_{M_{\dot{\alpha}}}\left[\frac{-p}{Z_d}\right] \tag{74}$$

$$m_{23} = (I_{ZZ} - I_{XX})r - 2pI_{XZ} - qI_{YZ} + QSdC_{M_{\dot{\alpha}}}\left[\frac{-\beta}{Z_d}\right] \tag{75}$$

$$m_{24} = rI_{XY} - pI_{YZ} + QSd\left[C_{m_q} + C_{N_{\dot{\alpha}}}\frac{1 + \tilde{Q}C_{N_q}}{Z_d}\right] \tag{76}$$

$$m_{25} = (I_{ZZ} - I_{XX})p + 2rI_{XZ} + qI_{XY} \tag{77}$$

$$n_{21} = 0 \tag{78}$$

$$n_{22} = QSd\left[C_{m_{\delta q}} + C_{N_{\dot{\alpha}}}\frac{Q\tilde{C}_{N_{\delta q}}}{Z_d}\right] \tag{79}$$

$$n_{23} = 0 \tag{80}$$

Finally, taking the partial derivatives of row 3 of Equation (62) with respect to each of the elements in **x** and u leads to

$$m_{31} = 0 \tag{81}$$

$$m_{32} = QSdC_{n_\beta} \tag{82}$$

$$m_{33} = (I_{XX} - I_{YY})q + 2pI_{XY} + rI_{YZ} + QSdC_{n_p} \tag{83}$$

$$m_{34} = (I_{XX}-I_{YY})p - 2qI_{XY} - rI_{XZ} \tag{84}$$

$$m_{35} = pI_{YZ} - qI_{XZ} + QSdC_{n_r} \tag{85}$$

$$n_{31} = QSdC_{n_{\delta p}} \tag{86}$$

$$n_{32} = 0 \tag{87}$$

$$n_{33} = QSdC_{n_{\delta r}} \tag{88}$$

Since the inertia matrix (J) is independent of the states and controls, the matrices **M** and **N** can now be multiplied by J^{-1}. The system matrices **A** and **B** can be written as

$$A = \begin{bmatrix} a_{11} & a_{12} & a_{13} & a_{14} & 0 \\ a_{21} & a_{22} & a_{23} & 0 & a_{25} \\ - & - & - & - & - & - & - & - \\ & & J^{-1}M & & \end{bmatrix} \tag{89}$$

$$B = \begin{bmatrix} 0 & b_{12} & 0 \\ b_{21} & 0 & b_{23} \\ - & - & - & - & - \\ & J^{-1}N & \end{bmatrix} \tag{90}$$

Equations (89) and (90) are in the form used to compute the linearized models for the selected design points.

2. LINEAR MODEL FOR SYSTEM 1

The linearized model for an altitude of 40,000 feet, mach 2.5, and angle-of-attack of 10 degrees is given by

$$A = \begin{bmatrix} -1.57 & 0.00 & 0.00 & 1.00 & 0.00 \\ 0.00 & -0.50 & 0.17 & 0.00 & -1.00 \\ -21.13 & -2876.70 & -2.10 & -0.14 & -0.05 \\ -82.92 & -11.22 & -0.01 & -0.57 & 0.00 \\ -0.19 & -11.86 & -0.01 & 0.00 & -0.57 \end{bmatrix} \tag{91}$$

and

$$B = \begin{bmatrix} 0.00 & -0.10 & 0.00 \\ -0.07 & 0.00 & 0.11 \\ -1234.70 & -30.49 & -1803.20 \\ -4.82 & -119.65 & -7.00 \\ 14.84 & 0.27 & -150.58 \end{bmatrix} \quad (92)$$

Sideslip angle, and body rates are all zero for this model. For purposes of example this model will be called linear system number 1.

3. LINEAR MODEL FOR SYSTEM 2

The linearized model for an altitude of 65,000 feet, mach 3.0, and angle-of-attack of 10 degrees is given by

$$A = \begin{bmatrix} -0.53 & 0.00 & 0.00 & 1.00 & 0.00 \\ 0.00 & -0.18 & 0.17 & 0.00 & -1.00 \\ -8.79 & -1010.94 & -0.62 & -0.05 & -0.07 \\ -34.50 & -3.94 & 0.00 & -0.18 & 0.00 \\ -0.08 & -6.03 & 0.00 & 0.00 & -0.19 \end{bmatrix} \quad (93)$$

$$B = \begin{bmatrix} 0.00 & -0.03 & 0.00 \\ 0.01 & 0.00 & 0.04 \\ -422.01 & -10.67 & -668.86 \\ -1.64 & -41.87 & -2.59 \\ 7.48 & -0.10 & -59.05 \end{bmatrix} \quad (94)$$

Sideslip angle, and body rates are all zero for this model. For purposes of example this model will be called linear system number 2.

SECTION V
DESIGN CONSIDERATIONS

A number of considerations play an important role during autopilot design. Angle limitations are placed upon the sideslip angle and angle-of-attack. The design must take into account the method for commanding the airframe such as BTT-180 or BTT-90. The actuators must also be considered since they too impact autopilot performance.

1. SIDESLIP ANGLE

The sideslip angle, β, must be limited to ± 5 degrees to limit the coupling into the roll and pitch channels. The commanded sideslip from the BTT logic is zero. The EMRAAT airframe has a strong tendency to return to zero (or near zero) sideslip so this condition is easily met. Commands for small sideslip angles may be desirable in terms of reducing undesirable effects from seeker-roll channel coupling, but this effect is not addressed in this project.

2. ANGLE-OF-ATTACK

The angle-of-attack, α, must be limited from between -5 degrees to +25 degrees. This is the range for which the aerodynamic data provided for the airframe is valid. Because of the airframe design and control surface configuration, negative angles-of-attack reduce the control effectiveness. The BTT logic therefore commands angles-of-attack from between 0 to +20 degrees.

3. BTT LOGIC

The BTT logic determines the manner in which the airframe should maneuver in response to guidance law commands. The BTT logic used in this study is designed to command the missile to roll about the velocity vector. To do this rate commands for roll, pitch, and yaw rates and angle commands for angle-of-attack and sideslip are provided to the autopilot. Using this BTT logic the response times for both the roll rate and angle of attack become important.

4. ACTUATOR MODEL

The actuator model, for each of the control surfaces, is a fifth order electro-mechanical model. Since three actuators are used, they comprise a 15 state actuator system. This system is left out of the autopilot design. It is important that the bandwidth of the actuators be as high as possible, to accommodate the autopilot, while not being so high that rate limiting occurs within the actuators. The bandwidth for these actuators is 27 Hz.

5. ADDITIONAL CONSIDERATIONS

This study addresses only the missile rigid body. If the problem of the missile flexible modes were to be addressed then bandwidth restrictions on the controller become more severe since it is desirable to attenuate these modes.

The design is done for the case when the fuel has been exhausted. This simplifies the approach in that changing missile mass and the changing center of mass are not considered. All simulations of the design assume near-intercept conditions which also means the fuel supply is exhausted (or nearly exhausted). This is a good point to start the design since it is in near-intercept conditions where the autopilot performance is most critical. One of the next steps in the design is to include the case of a thrusting motor with changing missile mass. The thrusting motor is not within the scope of this thesis.

The design must address the fact that the autopilot is a digital implementation in a microprocessor. The autopilot receives discrete commands from the guidance law at a rate of 100 Hz and provides discrete commands for the actuators at the same rate. Also of concern is the computational delay which is from the time the guidance law commands the autopilot to the time the autopilot commands the actuators. The estimated computational delay is 6 mS.

SECTION VI

APPROACH

1. LINEAR REGULATOR MODEL

Figure 8 shows a simplified model of the missile control system. It should be noted that the guidance law, BTT logic, and seeker require more information about the missile dynamics than is shown in Figure 8. The figure is intended to show the interrelationship of the controller to the other systems and the airframe dynamics. The autopilot consists of the BTT logic and controller (with a gain schedule implemented).

The function of the BTT logic is to transform the lateral acceleration commands from the guidance law to commands that relate to controlling the airframe. In this approach the BTT logic generates angle rate commands for roll, pitch and yaw, and angle commands for angle-of-attack and sideslip. The BTT logic diagram is shown in Figure 9 (Reference 7). The BTT logic works well for this problem, so no work is done with this.

The controller is designed using linearized quadratic regulator (LQR) methods and is based on the linearized model from Section IV which is linearized about specific flight conditions and then discretized about a sample rate of 10 ms. The design also takes into account a computational delay of 6 ms. A simplified diagram of the regulator is shown in Figure 10. The rest of this section develops the regulator shown in Figure 10. Since the true system model is nonlinear and the flight conditions vary constantly, gain scheduling is implemented to develop a piecewise linear regulator.

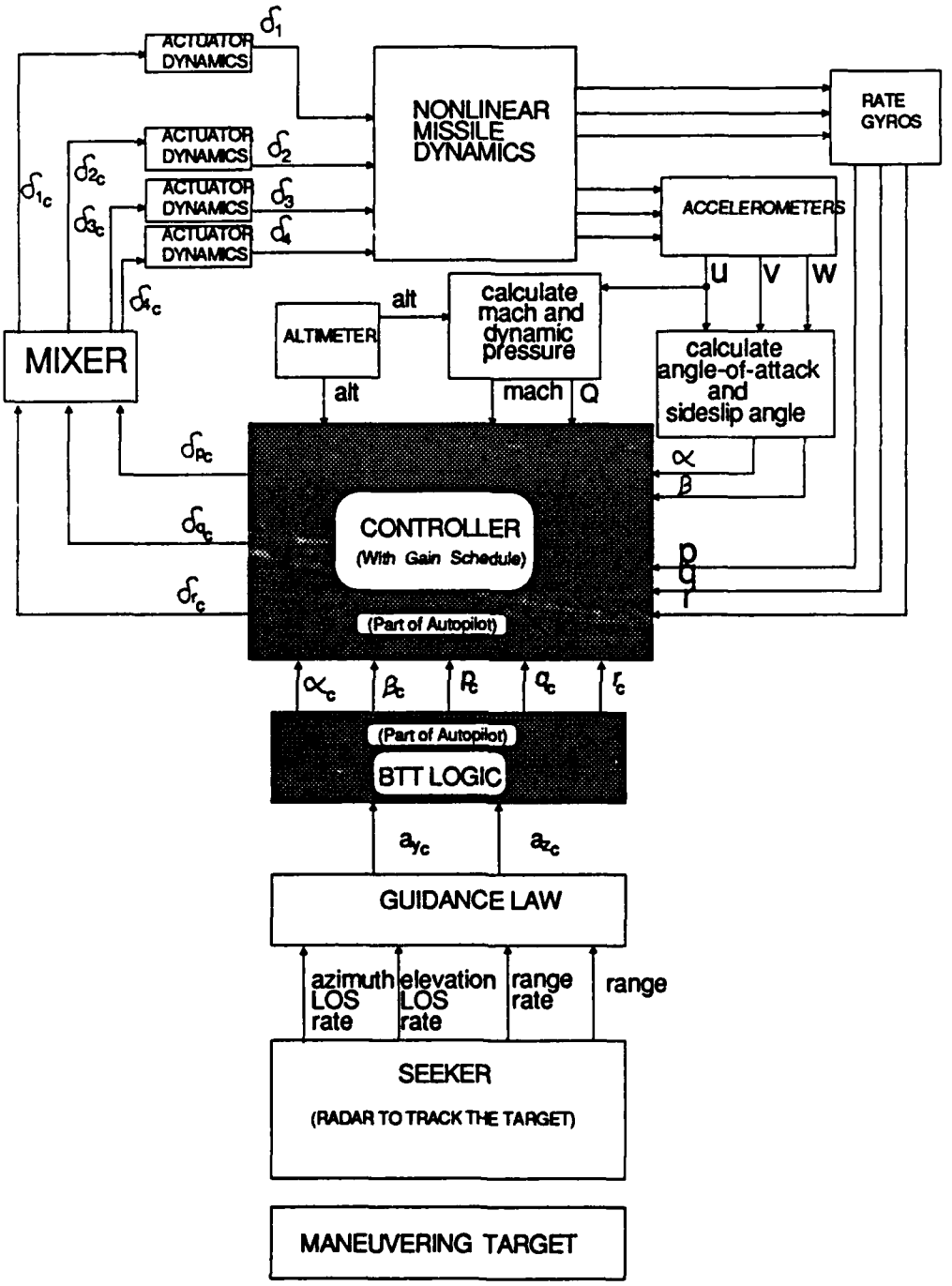

Figure 8. Missile System Block Diagram

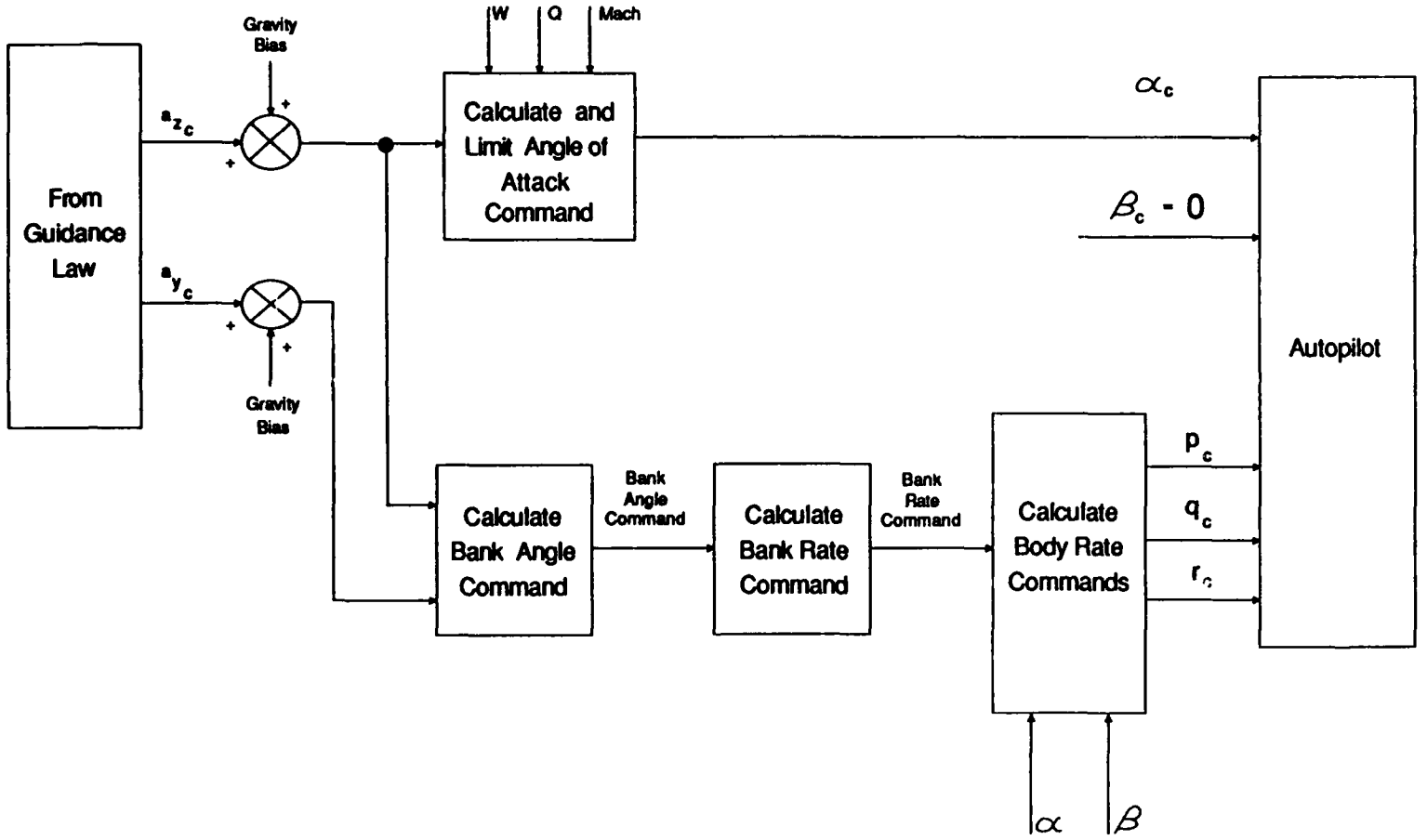

Figure 9. BTT Logic

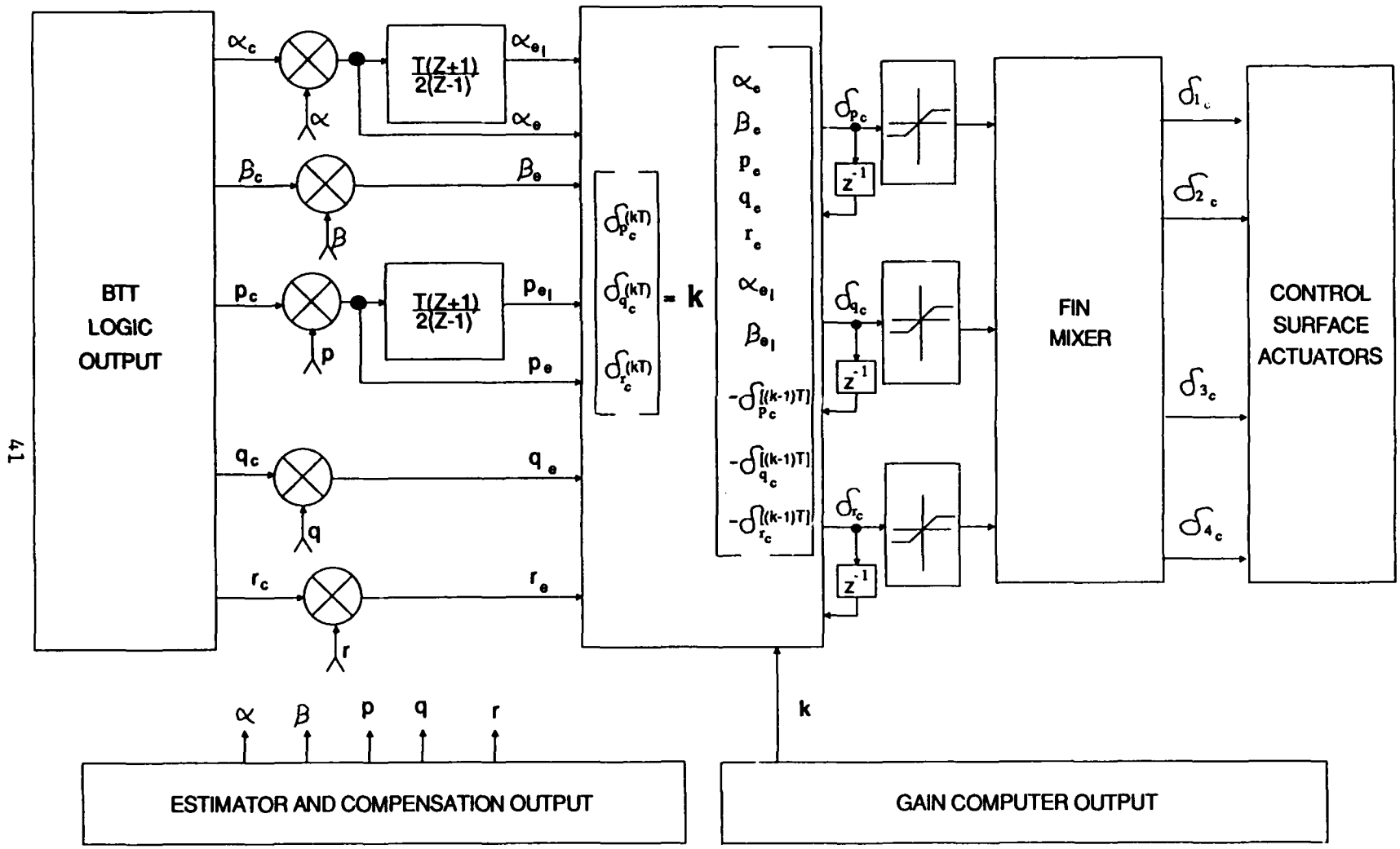

Figure 10. Discrete Linear Regulator

2. LINEAR QUADRATIC REGULATOR DESIGN

Of the five states in $\mathbf{x}$, α, β and p require more precise control than q and r. As was previously explained in Section V, there is no problem in controlling β. The linear model is augmented with integral states for α and p to minimize their steady-state errors and improve command tracking. The augmented system can be specified as:

$$\mathbf{x}_I = \left[\mathbf{x} \;\middle|\; \alpha_I \quad p_I\right]^T \tag{95}$$

Where α_I and p_I are a time integration of the states α and p. The System matrices A and B are augmented with zeros and ones to include the new states. This leads to

$$\mathbf{A}_I = \left[\begin{array}{ccccc|cc} & & & & & 0 & 0 \\ & & & & & 0 & 0 \\ & & \mathbf{A} & & & 0 & 0 \\ & & & & & 0 & 0 \\ & & & & & 0 & 0 \\ \hline 1 & 0 & 0 & 0 & 0 & 0 & 0 \\ 0 & 0 & 1 & 0 & 0 & 0 & 0 \end{array}\right] \tag{96}$$

$$\mathbf{B}_I = \left[\begin{array}{ccc} & \mathbf{B} & \\ \hline 0 & 0 & 0 \\ 0 & 0 & 0 \end{array}\right] \tag{97}$$

In the LQR approach the optimal control for u is:

$$\mathbf{u} = -\mathbf{K}\,\mathbf{x} \tag{98}$$

Where K is the gain matrix. Transmission zero weighting is used to specify the quadratic weighting matrices Q and R for the performance index (Reference 12):

$$J = \int_0^\infty \left(x^T Q\, x + u^T R\, u \right) dt \tag{99}$$

In this approach, the same number of outputs are specified as are inputs. Transmission zeros are specified in a manner to introduce performance criteria. In the resulting closed loop system as the loop gain increases from a very small value, the eigenvalues for the closed loop system migrate from the open loop system eigenvalues to the transmission zeros. Following is a description of the approach used in Reference 7, but modified for this problem. The advantage of this approach is the ability to specify, to some extent, the structure of the the closed loop system eigenvalues using classical performance parameters such as damping factors and natural frequencies. In Reference 7, two regulators were designed, one for the pitch autopilot and one for the yaw/roll autopilot. The approach is modified for one regulator design for a roll/pitch/yaw autopilot.

For the state vector

$$x_I = \left[\alpha \quad \beta \quad p \quad q \quad r \quad \alpha_I \quad p_I \right]^T \tag{100}$$

the output vector y is selected to be

$$y = \left[y_\alpha \quad y_\beta \quad y_p \right]^T \tag{101}$$

Where the elements y_a, y_b, and y_p are determined in accordance with the autopilot designs in Reference 7. The same numbers are used for y_a, y_b, and y_p as in Reference 7 since the autopilots in Reference 7 are used

for comparison of performance. The linear system given in Equations (91) and (92) is used for this description. The first element in Equation (101) to be specified is y_α. From Reference 7 this first starts in the s-plane, and is written as

$$Y_\alpha(s) = \left[\frac{s^2 + a_\alpha s + b_\alpha}{s} \right] \alpha(s) \tag{102}$$

In the time domain

$$y_\alpha = \dot{\alpha} + a_\alpha \alpha + b_\alpha \alpha_I \tag{103}$$

Next $\dot{\alpha}$ is found from the linearized state equations to be

$$\dot{\alpha} = -1.6\alpha + q + - 0.1\delta_q \tag{104}$$

Where the coefficients of Equation (104) are the coefficients of the linear system matrices A and B in Equations (91) and (92). The coefficient for the control δ_q is neglected since it is small. Equation (104) is now substituted into Equation (103) to yield

$$y_\alpha = (-1.6 + a_\alpha)\alpha + q + b_\alpha \alpha_I \tag{105}$$

In Reference 7, $Y_b(s)$ is specified as

$$Y_\beta(s) = (s + a_\beta)\beta(s) \tag{106}$$

In the time domain

$$y_\beta = \dot{\beta} + a_\beta \beta \tag{107}$$

Where from the linearized state equations

$$\dot{\beta} = -0.5\beta + 0.2p - r \tag{108}$$

It follows that

$$y_\beta = (-0.5 + a_\beta)\beta + 0.2p - r \tag{109}$$

As done in Reference 7, the last element of Equation (101) is specified as

$$Y_p(s) = \left[\frac{(s + a_p)}{s} \right] p(s) \tag{110}$$

In the time domain:

$$y_p = p + a_p p_I \tag{111}$$

Equations (105), (109) and (111) now specify the elements of y in Equation (101). To find the weighting matrix Q, the output is defined as:

$$y = Cx \tag{112}$$

Next define Q to equal $0.01C^TC$ so that

$$y^Ty = 0.01x^TC^TCx = x^TQx \tag{113}$$

Where C^TC is scaled by 0.01 so it will be in the same numerical range as the control weighting matrix R, this leads to

$$Q = 0.01C^TC \tag{114}$$

The control weighting matrix R started with the control weighting matrices used in Reference 7. In Reference 7 the non-zero off diagonal elements in R were chosen to minimize control surface coupling. By trial and error, the diagonal elements of R were varied from those used in Reference 7 to achieve good performance with the autopilot operating in the presence of noisy measurements. This choice leads to less than optimal deterministic performance. The matrix R as used for this problem is:

$$R = \begin{bmatrix} 10.2 & 0 & 1.8 \\ 0 & 2.5 & 0 \\ 1.8 & 0 & 9.2 \end{bmatrix} \tag{115}$$

Table 1 lists the transmission zeros used for this design and specifies the coefficients for Equations (105), (109) and (111).

TABLE 1. TRANSMISSION ZEROS USED FOR LINEAR SYSTEM 1

COEFFICIENTS(S)	VALUE(S)	TRANSMISSION ZERO(S)
a_α and b_α	11.7 and 39.7	$s = -5.9 \pm j2.3$
a_β	5.5	$s = -5.5$
a_p	5.0	$s = -5.0$

Using the data from Table 1 in Equations (105), (109), (111) and using Equation (114) to scale Q, leads to:

$$Q = \begin{bmatrix} 1.0 & 0.0 & 0.0 & 0.1 & 0.0 & 4.0 & 0.0 \\ 0.0 & 0.3 & 0.0 & 0.0 & -0.1 & 0.0 & 0.0 \\ 0.0 & 0.0 & 0.0 & 0.0 & 0.0 & 0.0 & 0.1 \\ 0.1 & 0.0 & 0.0 & 0.0 & 0.0 & 0.4 & 0.0 \\ 0.0 & -0.1 & 0.0 & 0.0 & 0.0 & 0.0 & 0.0 \\ 4.0 & 0.0 & 0.0 & 0.4 & 0.0 & 15.7 & 0.0 \\ 0.0 & 0.0 & 0.1 & 0.0 & 0.0 & 0.0 & 0.3 \end{bmatrix} \quad (116)$$

Table 2 lists the eigenvalues for the open and closed loop system based on an LQR design for linear system number 1 (the linear model in Figure 8). Also included in Table 2 are eigenvalues for the closed loop system for a large loop gain to show that in fact as the loop gain is increased the eigenvalues do migrate to the transmission zeros. The large loop gain is accomplished by reducing R by a large scale factor.

TABLE 2. OPEN AND CLOSED LOOP EIGENVALUES FOR LINEAR SYSTEM NUMBER 1

OPEN LOOP	CLOSED LOOP	LARGE LOOP GAIN
0.0 + j 0.0	- 2.8 + j 0.0	-5.0 + j 0.0
0.0 + j 0.0	- 5.1 + j 0.0	-5.5 + j 0.0
-0.6 + j 0.0	- 5.0 + j 9.0	-5.8 + j 2.4
-1.1 + j 9.1	- 5.0 - j 9.0	-5.8 - j 2.4
-1.1 - j 9.1	- 6.5 + j13.8	-10^9 + j 0.0
-1.3 + j22.1	- 6.5 - j13.8	-10^8 + j 0.0
-1.3 - j22.1	- 6.5 - j13.8	-10^8 + j 0.0

3. DISCRETE DESIGN

The approach takes into account that the autopilot is implemented digitally in a microprocessor. The autopilot update rate is 10 ms and there is a 6 ms computational delay between the autopilot commands and the actuator commands. The computational delay and update rate are shown in Figure 11. In the nonlinear 6-DOF missile simulation the control commands from the autopilot are delayed by 6 ms to simulate a digital implementation. The continuous linear system is discretized using the method in Reference 13. Following is a description of the method used to discretize the continuous system. The control, u(k), is specified as

$$u(k) = -Kx(k) \tag{117}$$

where u(k) is delayed by the computational delay τ. In Figure 11, the transition from k to k+τ, total time equal to τ, is given by

$$\mathbf{x}(k+\tau) = \Phi(\tau)\mathbf{x}(k) + \Gamma(\tau)u(k-1) \tag{118}$$

The transition from $k+\tau$ to $k+1$, total time equal to $T-\tau$, is given by

$$\mathbf{x}(k+1) = \Phi(T-\tau)\mathbf{x}(k+\tau) + \Gamma(T-\tau)u(k) \tag{119}$$

Substituting (118) for $\mathbf{x}(k+\tau)$ into (119) leads to

$$\mathbf{x}(k+1) = \Phi(T-\tau)\Phi(\tau)\mathbf{x}(k) + \Phi(T-\tau)\Gamma(\tau)u(k-1) + \Gamma(T-\tau)u(k) \tag{120}$$

which may be simplified to

$$\mathbf{x}(k+1) = \Phi(T)\mathbf{x}(k) + \Phi(T-\tau)\Gamma(\tau)u(k-1) + \Gamma(T-\tau)u(k) \tag{121}$$

To remove $u(k-1)$ from the right hand side of Equation (121), the state vector $\mathbf{x}_I$ is augmented with $u(k-1)$, this leads to the discrete state vector

$$\mathbf{x}_d = \begin{bmatrix} \mathbf{x}_I(k) \\ u(k-1) \end{bmatrix} \tag{122}$$

The discrete system in Equation (121) can now be written as:

$$\begin{bmatrix} \mathbf{x}(k+1) \\ u(k) \end{bmatrix} = \begin{bmatrix} \Phi(T) & \Phi(T-\tau)\Gamma(\tau) \\ 0 & 0 \end{bmatrix} \begin{bmatrix} \mathbf{x}_I(k) \\ u(k-1) \end{bmatrix} + \begin{bmatrix} \Gamma(T-\tau) \\ I \end{bmatrix} u(kT) \tag{123}$$

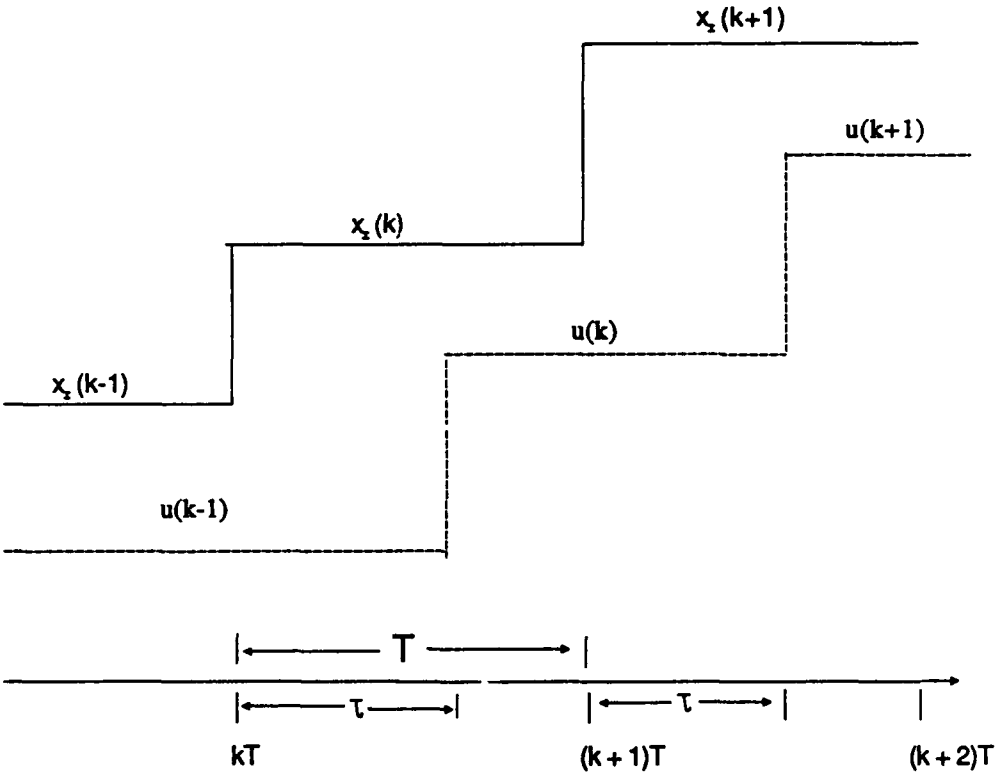

T = 0.010 Second

τ = 0.006 Second

T - τ = 0.004 Second

Figure 11. Computational Delay

Using this approach the linear model is augmented with the control commands for u(k-1). The previous control commands are used since these are known, and there are no direct measurements available for the controls. This is possible since the control actuators response time is faster than the autopilot regulator. This adds three states, so the discrete model now consists of 10 states. During the discrete LQR design no weighting is placed on the augmented states for the controls, the state weighting matrix Q is augmented with zeros. At this point, the new state vector is defined as

$$x_D = \left[\alpha\ \beta\ p\ q\ r\ \alpha_I\ p_I\ \delta_p\ \delta_q\ \delta_r\right]^T \tag{124}$$

4. GAIN SCHEDULING

a. Implementation Considerations

An important consideration of the design is to minimize the amount of gain scheduling and have large gain margins in the design. Since the model is linearized about specific flight conditions, gains must be scheduled to account for the other than nominal flight conditions. Gain scheduling can become an enormous burden on the digital implementation of the autopilot so it is desirable to limit the amount of gains that must be scheduled.

A brute force gain scheduling technique is too complex to implement and includes too many rapidly changing variables. For the problem of a constant mass model, and a discretized model, the gains may need to be scheduled against the following variables: α, β, p, q, r, δ_p, δ_q, δ_r, mach, and altitude. This indirectly includes dynamic pressure since dynamic pressure is a function of altitude and mach. There are 10 variables and 3 controls which means that a total of 30 gains will have to be scheduled. If mass were not assumed to be constant, it too would become part of the overall scheduling problem.

Normally, autopilot gains are implemented by scheduling them as a function of only a few variables. Typically, these are combinations of α, β, dynamic pressure, and mach. While other combinations may be used,

the scheduling is restricted still to a small number of variables. Some general rules of thumb can be applied to the gain scheduling problem.

First, it is desirable to schedule gains against slower changing parameters such as mach and dynamic pressure. This helps to maintain stability during the presence of rapidly changing guidance loop dynamics (primarily near intercept).

Second, since the implementation is discrete, new updates for gains will be introduced as small steps into the system resulting in some possible undesirable transient responses. This means it can be necessary to slow the rate at which the gains are calculated.

Third, it is possible to scale some gains against a slowly changing parameter such as dynamic pressure. Other relationships between the gains and variables if identified can be exploited. Gains that only undergo small variations can be fixed as constant. Gains that have little contribution can possibly be ignored.

Finally, large gains margins are desirable for the designs at the nominal conditions so the system is likely to be stable when it is not at the nominal operating points. This helps in terms of reducing the amount of gains that must be scheduled. The goal set for the nominal design is to have gain margins of at least 6dB and phase margins greater than 30 degrees.

b. Gain Schedule.

The gain scheduling approach used here involves the random generation of 500 linear models over a number of flight conditions, using the nominal flight condition as the mean of a multivariate uniform distribution. The mean components and distribution endpoints are shown in Table 3. Figure 12 summarizes the gain scheduling approach. For each randomly selected flight condition a discrete LQR design is performed based on the resulting linear model. The discrete LQR designs are then evaluated to assess the stability of the resulting closed loop controller for each design. Redesign is carried out if required. For this particular application, all designs were found to be stable and met the desired gains and phase margins.

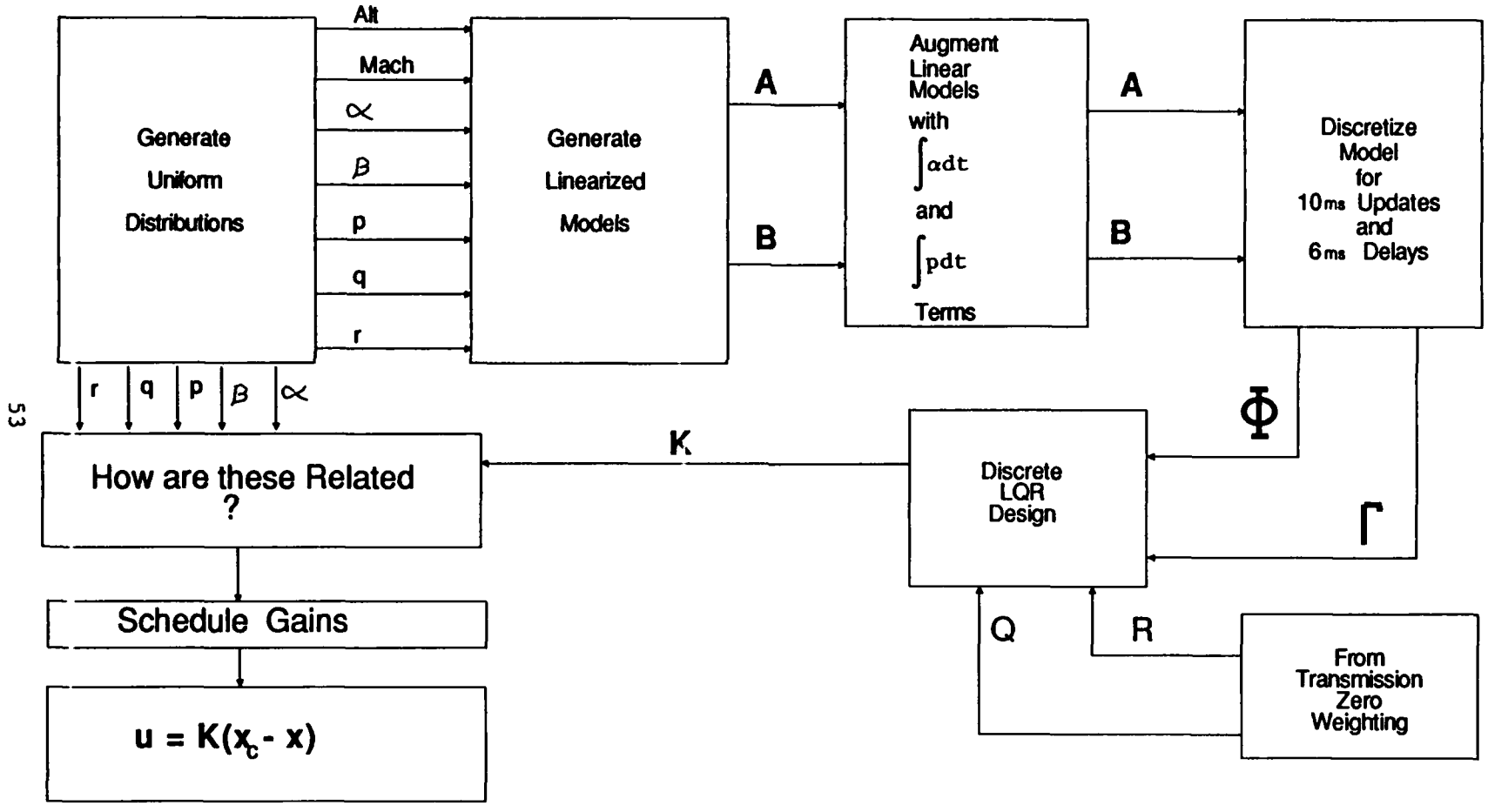

Figure 12. Gain Scheduling Approach

TABLE 3. FLIGHT CONDITIONS DISTRIBUTIONS USED IN THE INITIAL REGULATOR DESIGN

VARIABLE	MEAN	±
α (degrees)	10	15
β (degrees)	0	8
p (degrees/second)	0	800
q (degrees/second)	0	400
r (degrees/second)	0	400
altitude (feet)	40,000	0
mach	2.5	0

5. MACH 2.5, AND 40,000 FOOT DESIGN

As shown in Table 3, the nominal flight conditions are at mach 2.5, 40,000 feet altitude, and angle-of-attack of 10 degrees. A discrete LQR design for the system linearized about the nominal flight condition was performed using the previously defined approach to specify the weighting matrices Q and R.

Figures 13, 14, and 15 are discrete bode plots for the nominal design. The frequencies used to generate the plots varied from 0.1 radians/second to 1000 radians/second. The plots are for the augmented discrete open loop system with the output specified as

$$\tilde{u} = K x_D \tag{125}$$

Where

$$\tilde{u} = \begin{bmatrix} \tilde{\delta}_p & \tilde{\delta}_q & \tilde{\delta}_r \end{bmatrix}^T \tag{126}$$

Figure 13 has for its input and output, δ_p and $\tilde{\delta}_p$. Figure 14 has for its input and output, δ_q and $\tilde{\delta}_q$. Figure 15 has for its input and output,

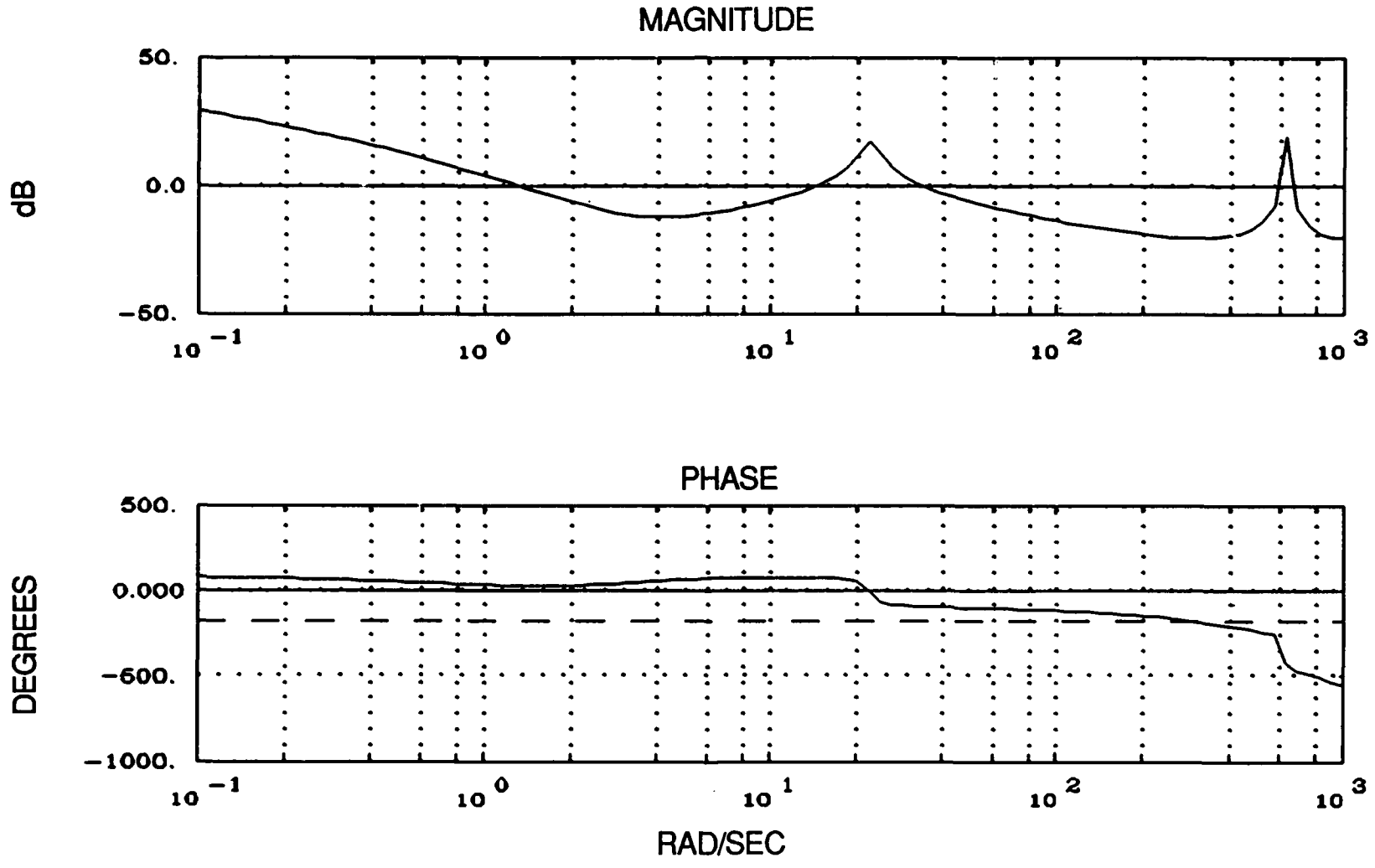

Figure 13. Discrete Bode Plot for System 1 (Aileron Loop)

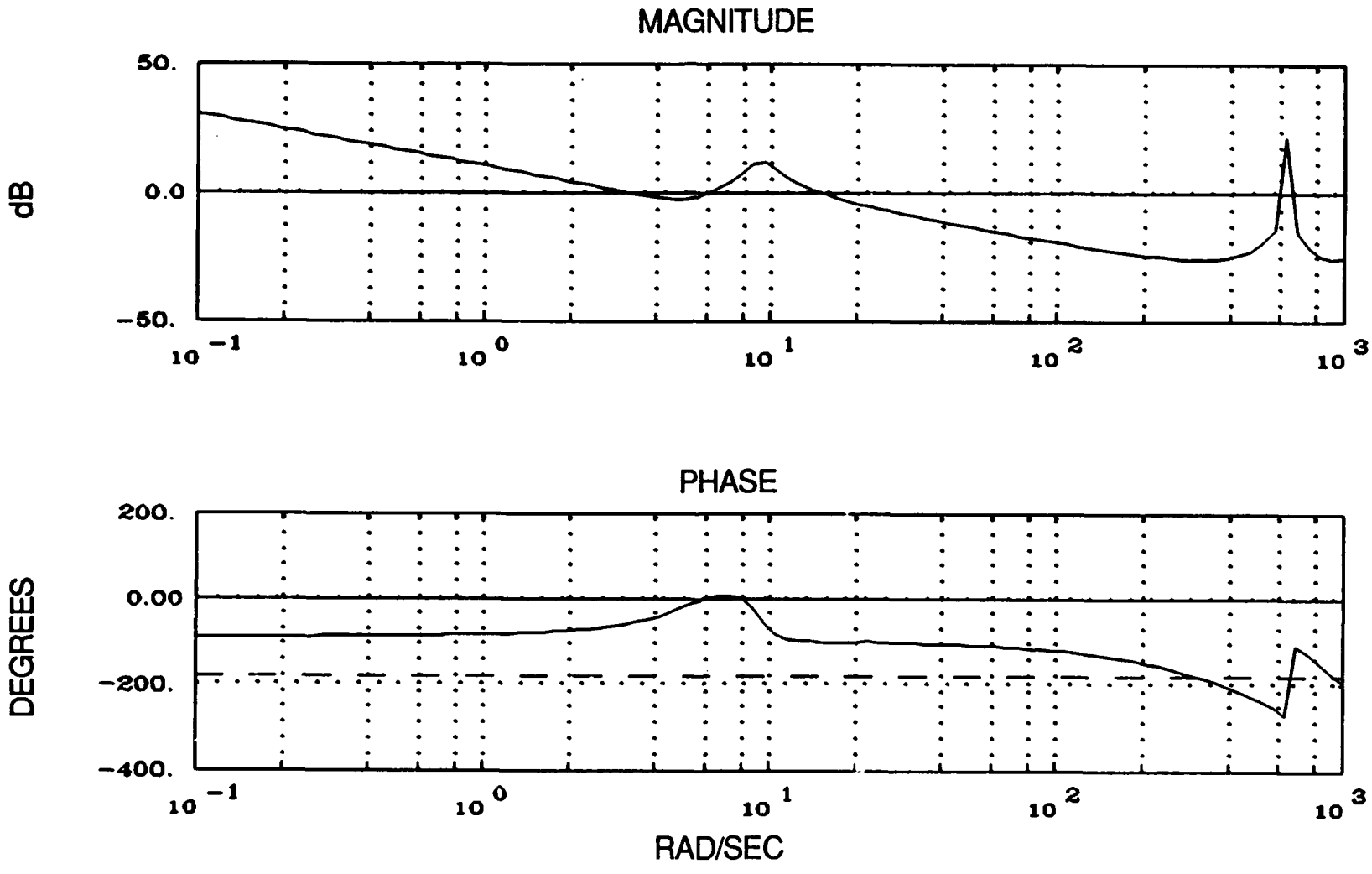

Figure 14. Discrete Bode Plot for System 1 (Elevator Loop)

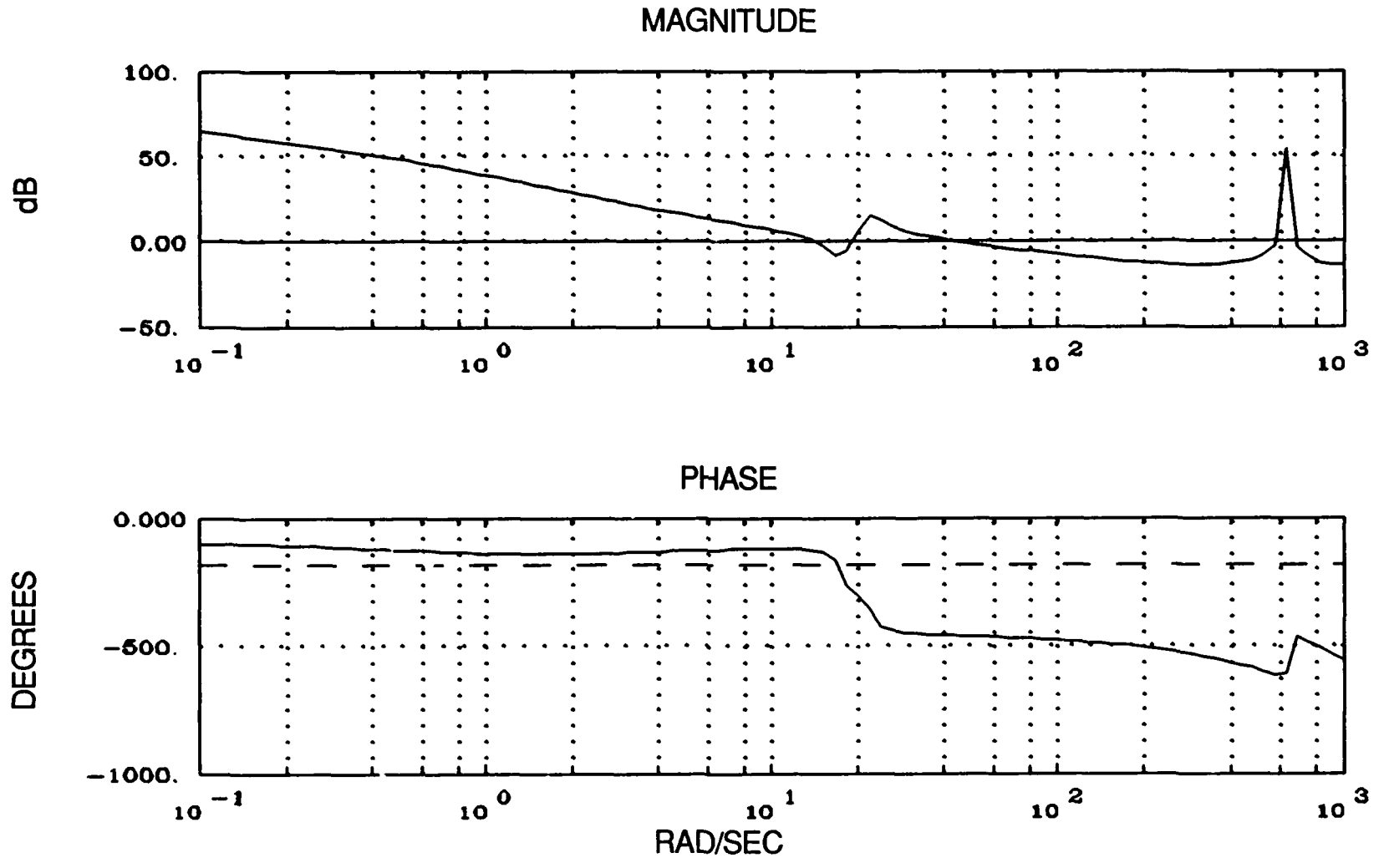

Figure 15. Discrete Bode Plot for System 1 (Rudder Loop)

δ_r and $\bar{\delta}_r$. Based on these plots it can be seen that the phase and gain margins for the nominal design have been met.

The next step was to assess the designs over the entire range of conditions shown in Table 3. Figures 16 through 18 are plots for the gains based on the conditions in Table 3. Each plot was obtained by plotting the gains against the individual flight conditions in an attempt to observe any relationship between gains and the flight conditions. After a few tries it readily became apparent that most gains are primarily dependent on α or p. A few gains showed some dependence on r but these gains were small. In some cases there is a strong dependence of the gains on both α and p. Following is a brief summary of Figures 16 - 18.

In Figure 16 (B, C, E, H, and J), Figure 17 (A, D, I, and J), and Figure 18 (B, C, E, H, and J) a strong relationship between α and the gains appears to exist. Figures 16 G and 18 G, show some correlation to α. Very little correlation could be discerned between any of the variables and Figures 16 (G) and 18 (G).

Figure 16 (F), Figure 17 (F), and Figure 18 (F) all show a strong relationship to the roll rate (p). In Figure 16 (A, D,and I), Figure 17 (B and E), and Figure 18 (A and D) although plotted against one variable, it appeared during plotting the gains, that a relationship exists between these gains and α and p. In the plots where a relationship appears to exist between the gain and the yaw rate (r), Figure 17 (C, G, H, and J), and Figure 18 (D and I), it also appears that these gains when multiplied by their corresponding variables will be negligible.

It is interesting to note that the gains that vary as a function of p, or a combination of α and p, tend to vary linearly with p. This is not readily obvious from some of the figures presented; however, while plotting these gains against different variables the relationship does occur. This is a useful result since p is a rapidly changing variable. Now it appears that scheduling against p may not pose problems. The only real exception to this is Figure 17 (F); however, in this figure the gain appears very close to having a linear relationship with roll rate. To isolate and identify these gains, 200 designs were performed

using the conditions in Table 4. Results of these designs, although not shown, verify the assumptions made about Figures 16 through 18.

TABLE 4. FLIGHT CONDITIONS DISTRIBUTIONS USED IN THE FINAL REGULATOR DESIGN

VARIABLE	MEAN	±
α (degrees)	10	15
β (degrees)	0	0
p (degrees/second)	0	800
q (degrees/second)	0	0
r (degrees/second)	0	0
altitude (feet)	40,000	0
mach	2.5	0

From the designs based on Table 4, it is possible to assume that for a given altitude and mach the gains need only be scheduled against α and p. In most cases the gains need only be scheduled against α. This considerably simplifies the approach to gain scheduling. Now simple table look-ups can be used for gain scheduling where the independent variables are α and p.

Another result obtained from Figures 16 through 18 is the interdependence of the roll and yaw dynamics, and independence of the pitch dynamics from the yaw and roll dynamics. This is an interesting result since autopilot studies usually begin with simplifying the nonlinear model and then linearizing the simplified model. For the EMRAAT airframe, approaches have either separated the model into pitch and yaw/roll dynamics or separated the model into roll and pitch/yaw dynamics. From the figures it appears that a reasonable approach is to separate the model into pitch dynamics and yaw/roll dynamics. The model for the yaw/roll dynamics should possibly include α and α_I as states. The approach for this problem does not separate the dynamics of the model. Separating the dynamics of the model is a potential topic for further work since it leads to a simpler implementation.

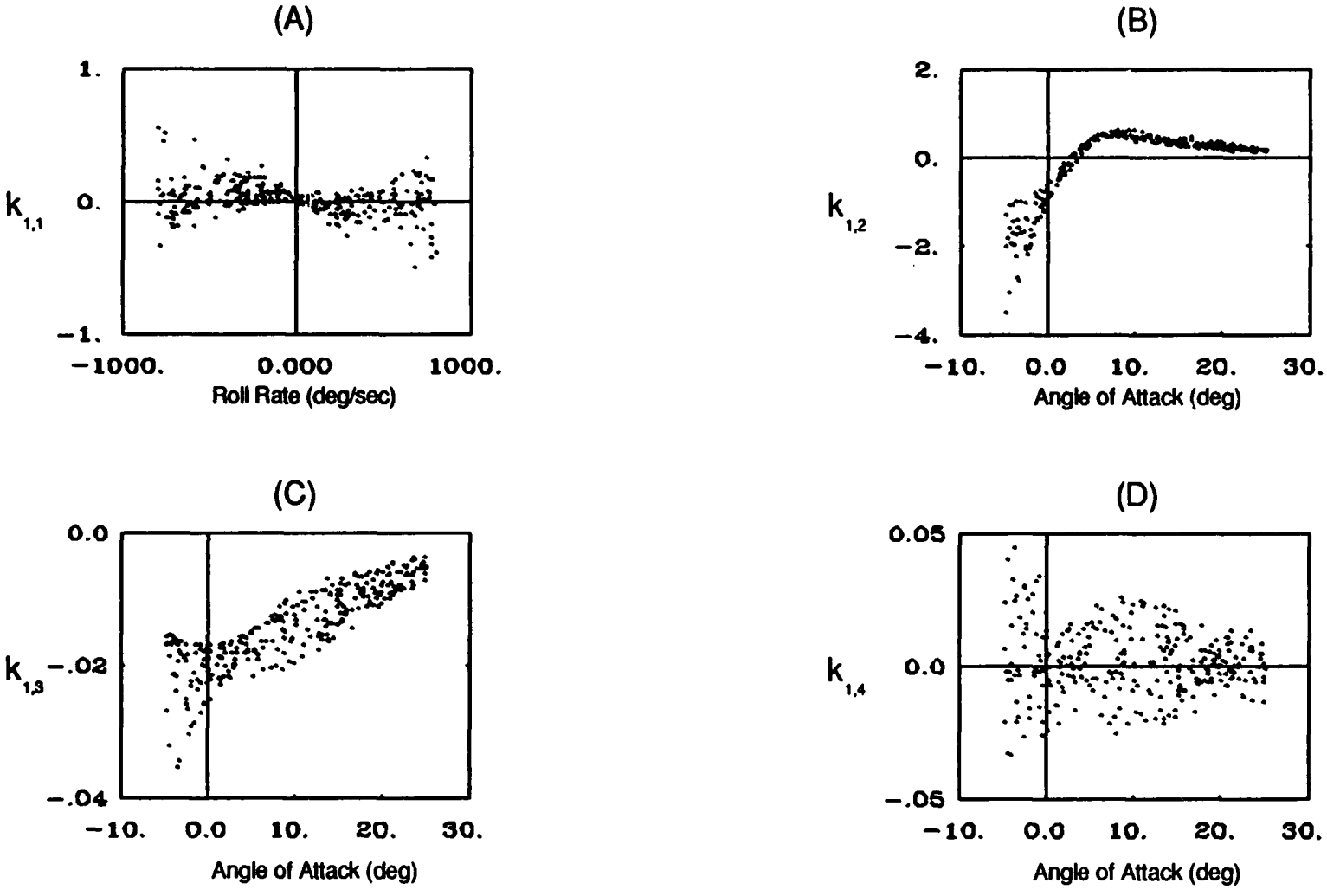

Figure 16. Correlation Plots for Aileron Gains

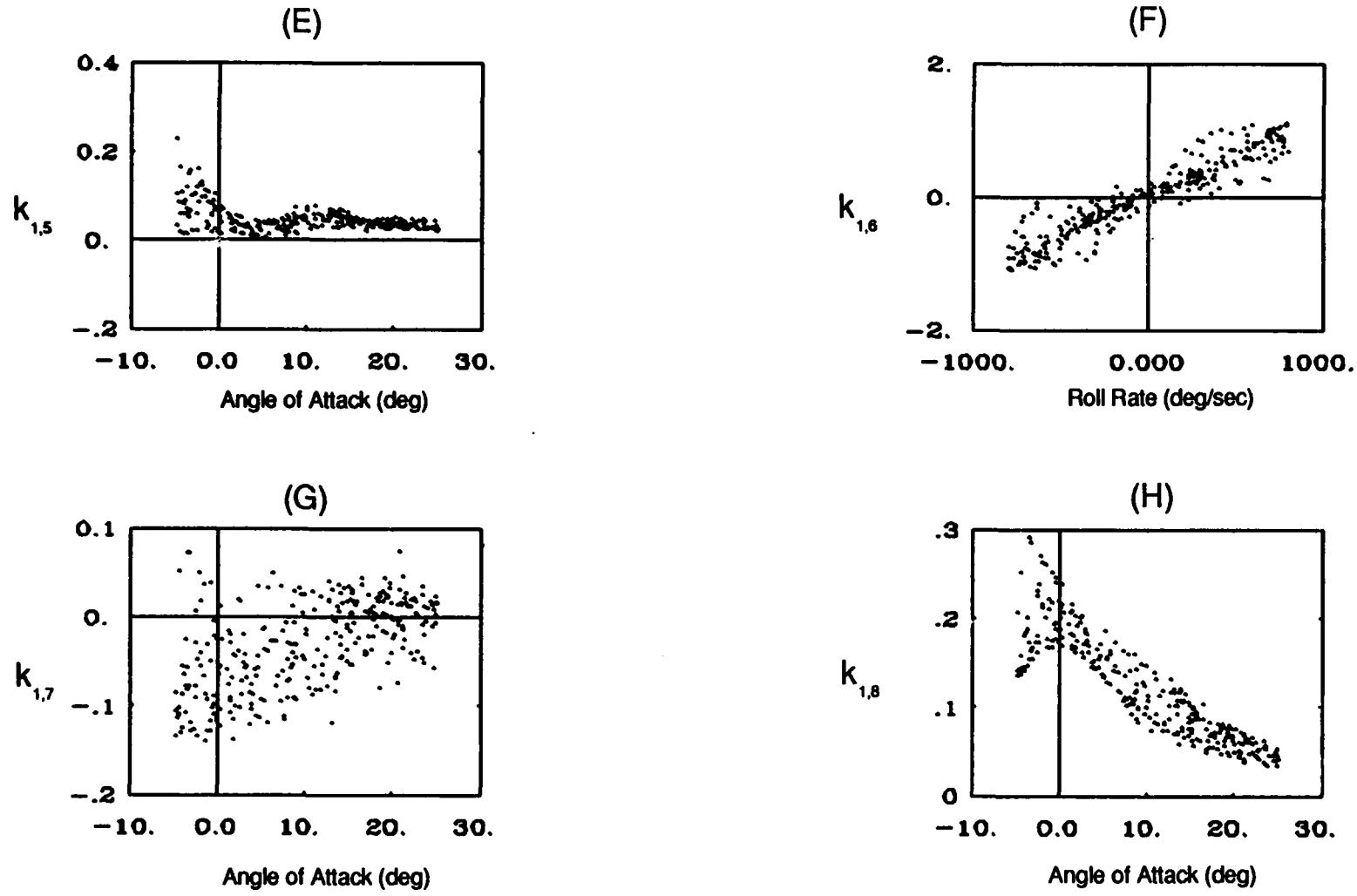

Figure 16. Correlation Plots for Aileron Gains (Continued)

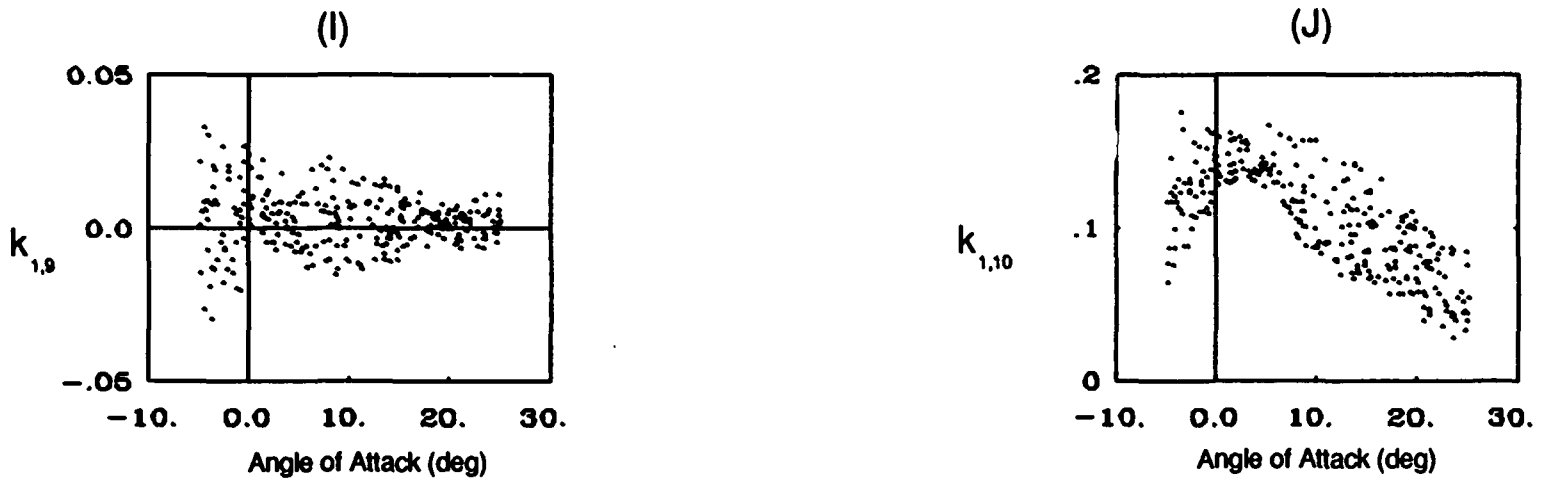

Figure 16. Correlation Plots for Aileron Gains (Concluded)

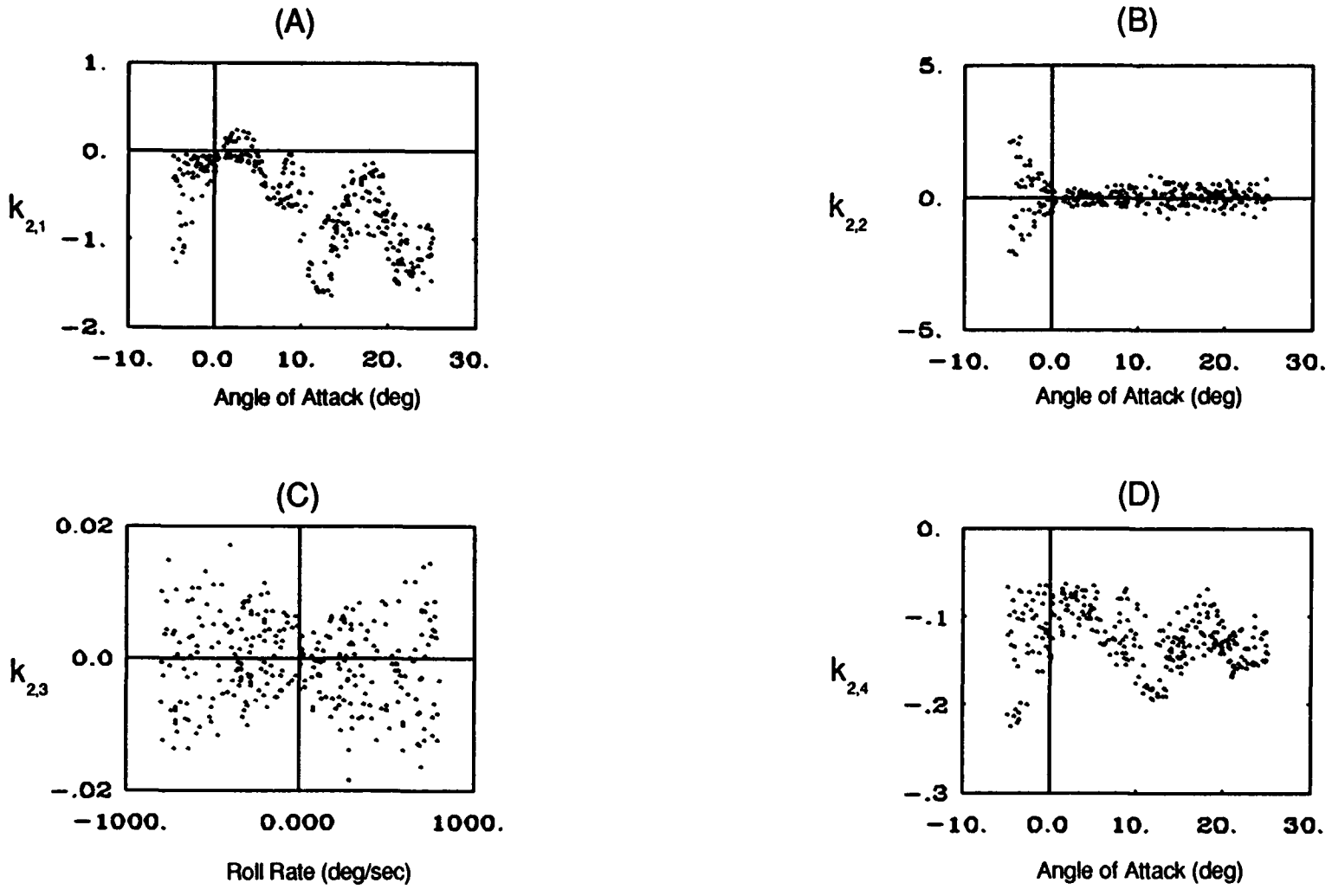

Figure 17. Correlation Plots for Elevator Gains

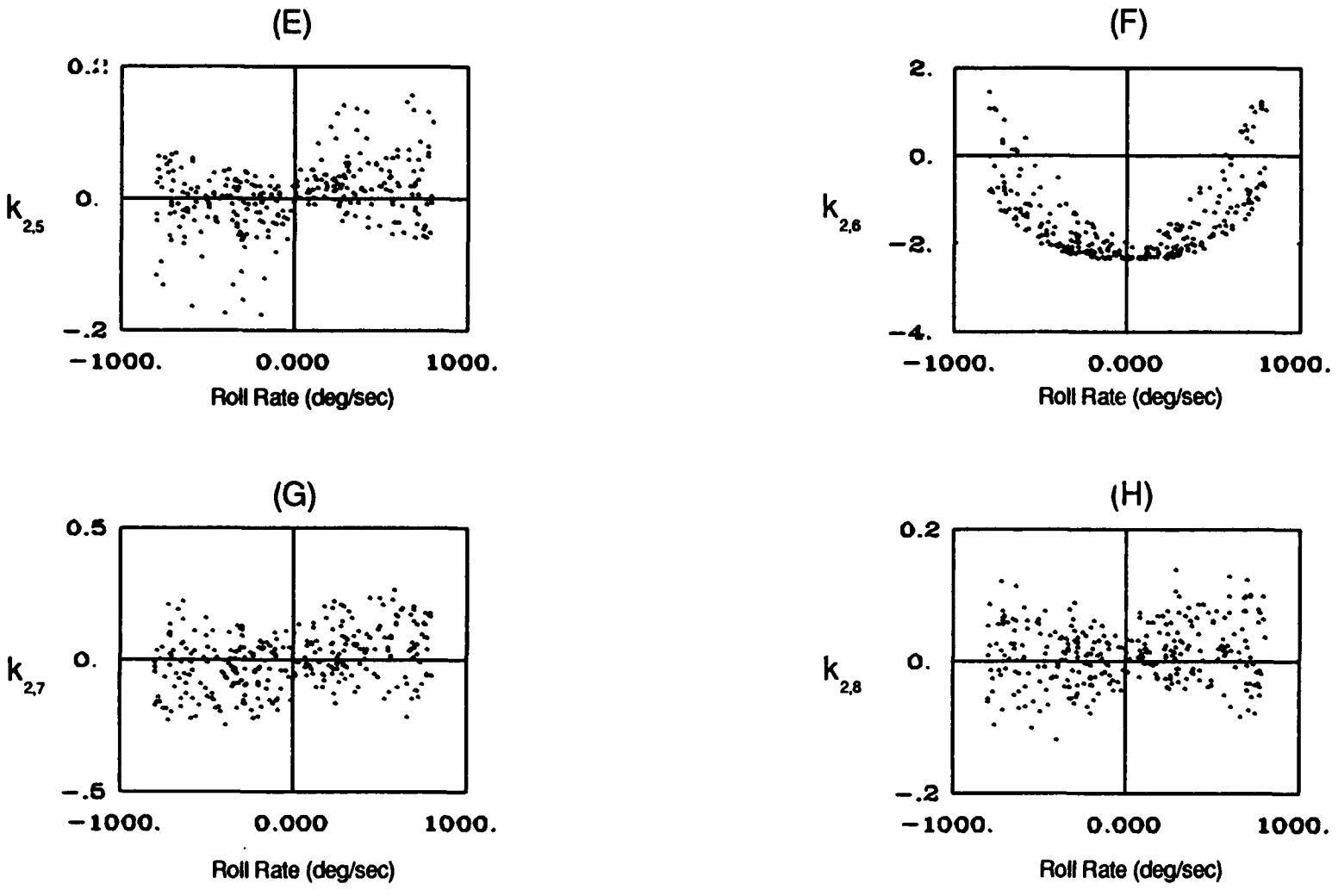

Figure 17. Correlation Plots for Elevator Gains (Continued)

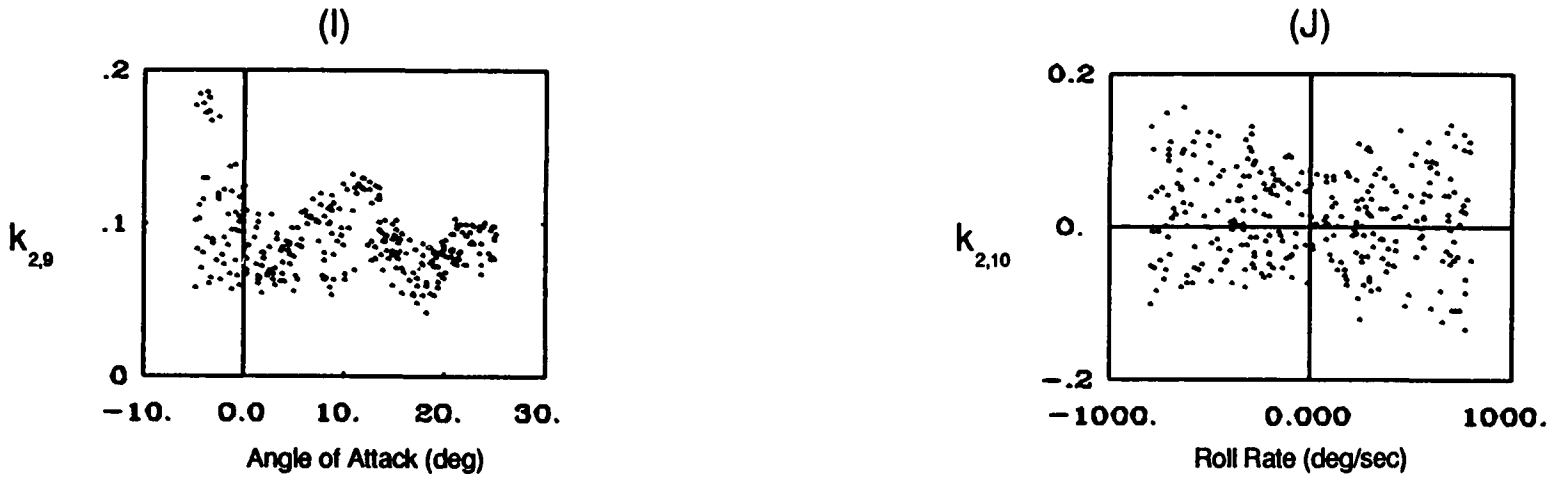

Figure 17. Correlation Plots for Elevator Gains (Concluded)

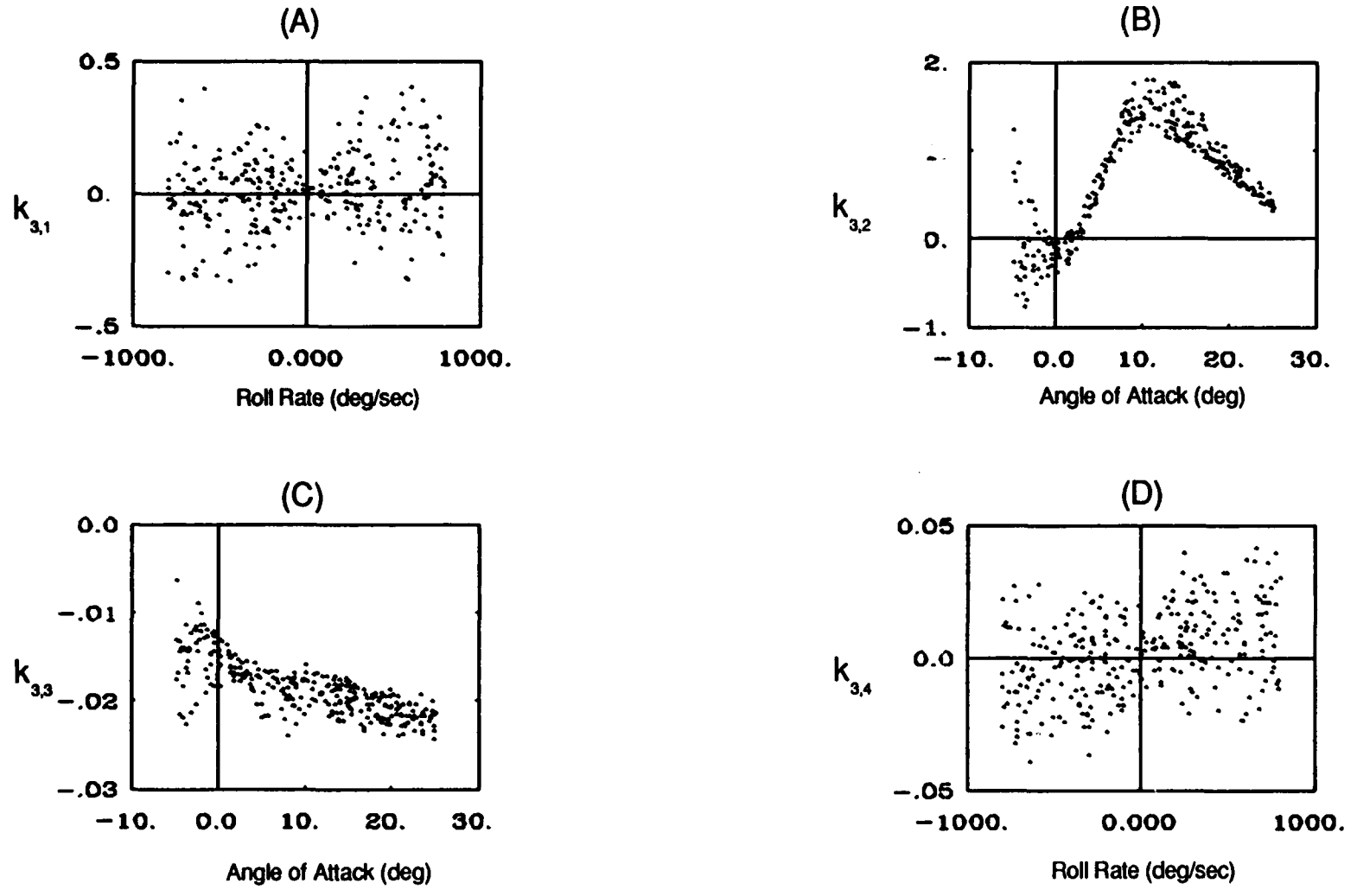

Figure 18. Correlation Plots for Rudder Gains

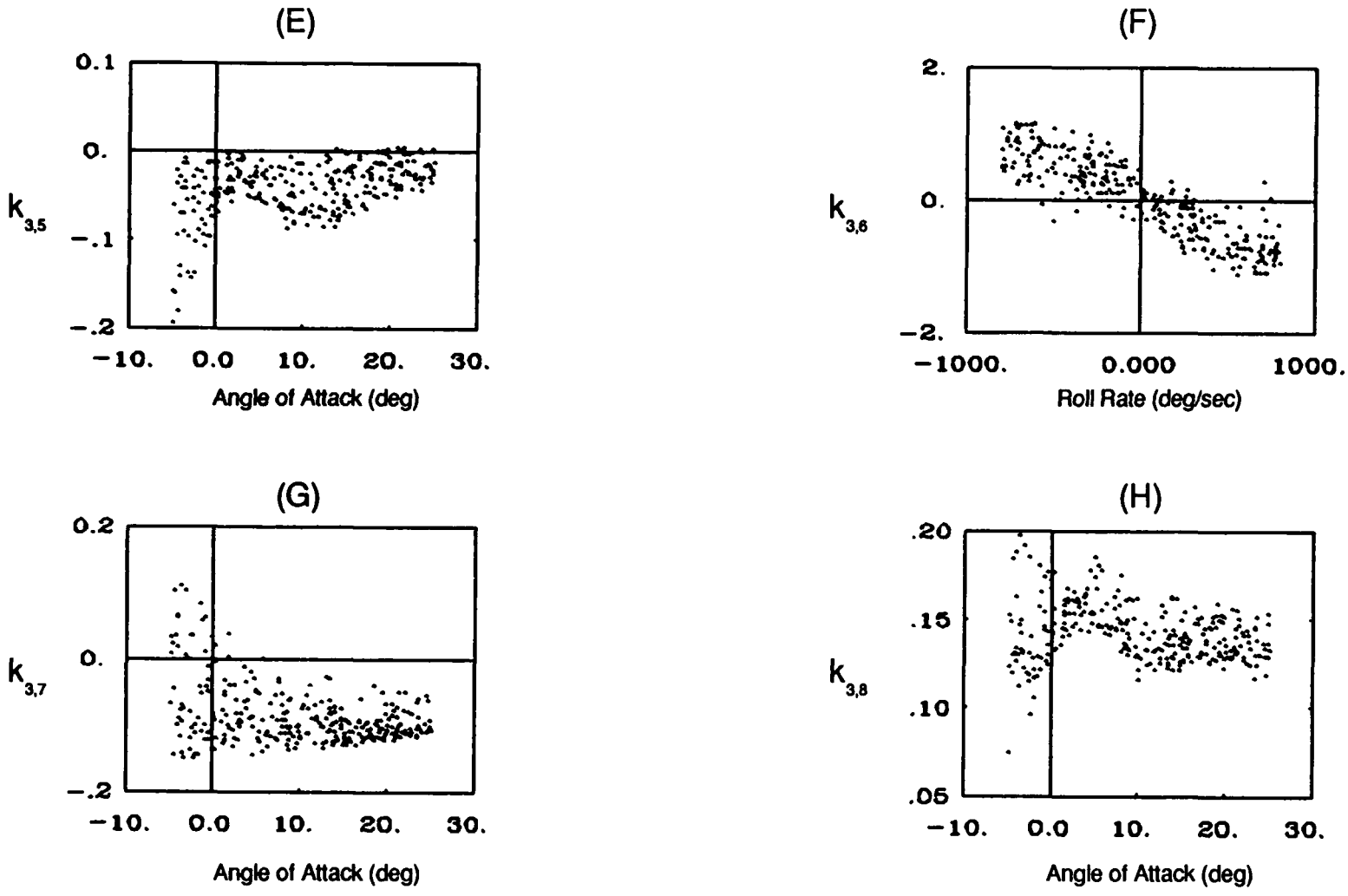

Figure 18. Correlation Plots for Rudder Gains (Continued)

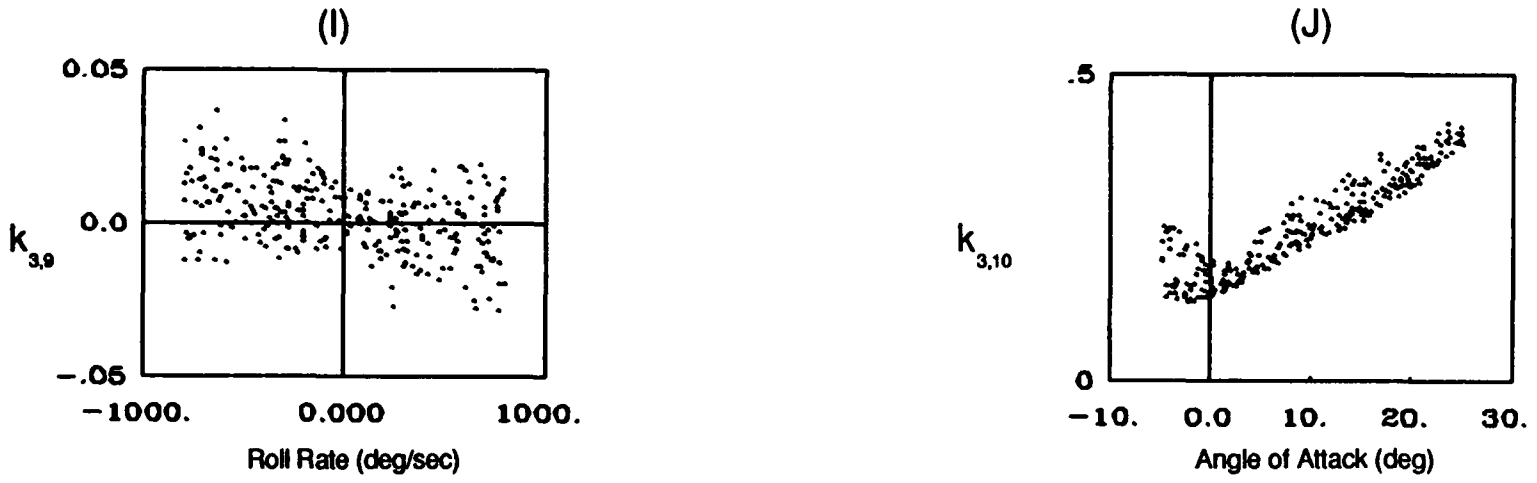

Figure 18. Correlation Plots for Rudder Gains (Concluded)

To assess the importance of the gains on α and α_I for the aileron and rudder commands, both a continuous and discrete design for the nominal flight condition were performed with the roll-rate changed to 600 degrees/sec. First, the closed loop eigenvalues for both the continuous and discrete systems were computed. Next, the aileron and elevator gains on α and α_I were set to zero. With the new set of gains, the closed loop eigenvalues were computed. Table 5 contains these results.

As can be seen in Table 5, the aileron and rudder gains on α and α_I appear to have a significant impact on the continuous closed loop eigenvalues. The discrete closed loop eigenvalues do show that one of the eigenvalues has moved closer to the unit circle for the case when the two gains were forced to zero. In the gain schedules all of the gains are retained and none are forced to zero.

To implement the gain schedules, the conditions in Table 4 were varied using an increment of 1 degree for alpha and an increment of 400 degrees/sec for p. This leads to 155 point designs. For simplicity these designs are scheduled using simple 2-dimensional linear table look-ups.

TABLE 5. COMPARISON OF EIGENVALUES

CONTINUOUS SYSTEM CLOSED LOOP EIGENVALUES
-2.0 + j1.6
-2.0 - j1.6
-4.9 + j0.0
-12.6 + j0.0
-8.2 + j23.8
-8.2 - j23.8
-60.8 + j 0.0
CONTINUOUS SYSTEM CLOSED LOOP EIGENVALUES (α and α_I terms for the aileron and and rudder set to zero)
-0.7 + j0.0
-3.8 - j0.0
-5.1 + j0.0
-12.8 + j0.0
-7.8 + j23.8
-7.8 - j23.8
-60.8 + j 0.0
DISCRETE SYSTEM CLOSED LOOP EIGENVALUES
0.00 + j0.00
0.00 + j0.00
0.00 + j0.00
0.53 + j0.00
0.88 + j0.00
0.89 + j0.22
0.89 - j0.22
0.95 + j0.00
0.98 + j0.02
0.98 - j0.02
DISCRETE SYSTEM CLOSED LOOP EIGENVALUES (α and α_I terms for the aileron and and rudder set to zero)
0.00 + j0.00
0.00 + j0.00
0.00 + j0.00
0.53 + j0.00
0.89 + j0.00
0.90 + j0.22
0.90 - j0.22
0.95 + j0.00
0.96 + j0.00
0.99 - j0.00

6. MACH 3.0, AND 65,000 FOOT DESIGN

The autopilot was redesigned using the previously described approach, but now for mach 3.0, at 65,000 feet. For the nominal design, the linear system in Figure 9 is used. This leads to a new state weighting matrix Q. A new control weighting matrix was also specified as

$$R=\begin{bmatrix} 6.2 & 2\,0 & 1.8 \\ 0 & 2.5 & 0 \\ 1.8 & 8\,0 & 8.2 \end{bmatrix} \tag{127}$$

Table 6 contains the discrete open and closed loop eigenvalues for the system of Equations (93) and (94). The same procedure for gain scheduling was performed as was done for the mach 2.5, 40,000 foot case. When plotting gains little or no change was observed in the way the gains were correlated to α and p. There is however, a little more dispersion of the points in some of the plots. This dispersion can be attributed to the higher altitude, which leads to a lower dynamic pressure. The lower dynamic pressure reduces the effectiveness of the controls and reduces the magnitude of the aerodynamic derivatives. Once this happens, coriolis and gyroscopic coupling effects become more pronounced.

TABLE 6. DISCRETE EIGENVALUES FOR SYSTEM NUMBER 2

DISCRETE SYSTEM OPEN LOOP EIGENVALUES
0.00 + j0.00
0.00 + j0.00
0.00 + j0.00
0.99 + j0.13
0.99 - j0.13
1.00 + j0.06
1.00 - j0.06
1.00 + j0.00
1.00 + j0.00
1.00 + j0.0C
DISCRETE SYSTEM CLOSED LOOP EIGENVALUES
0.00 + j0.00
0.00 + j0.00
0.00 + j0.00
0.81 + j0.00
0.95 + j0.00
0.95 + j0.08
0.95 - j0.08
0.98 + j0.00
0.98 + j0.06
0.98 - j0.06

SECTION VII
TESTING AND EVALUATION

1. AUTOPILOT USED FOR COMPARISON

For purposes of comparison, the autopilot in Reference 7 is used. The chief reason for this is both the autopilot in Reference 7 and the autopilot in this study use the same nonlinear simulation and the same Monte-Carlo simulation. The autopilot in Reference 7 will be referred to as the baseline autopilot.

2. ACCELERATION STEPS

Step commands for specified accelerations in the inertial reference frame were performed as shown in Table 7 for the mach 2.5, 40,000 foot design. This approach is a good method to assess autopilot performance since an inertial guidance step demands more from the autopilot than a step on one of the states in $\mathbf{x}$. It should be noted that more stressing maneuvers should be used for a complete analysis of performance, but for this study, only the four steps shown in Table 7 are used. In all four cases the missile initially assumes straight and level flight with an angle-of-attack that is sufficient to maintain trim (keep altitude constant). The steps are initiated at 1 second into flight.

In step number one, the vehicle is commanded to accelerate in only the inertial y-plane. Step 1 is the least complex maneuver of the four steps, however, the missile must bank about its velocity vector. To do this, the desired α must be achieved, and β must be kept to a minimum. In step 2, the missile is commanded to perform a 10 g dive. This forces the missile to bank 180 degrees about its velocity vector. Step 3 combines steps 1 and 2. In step 4, the missile is commanded to accelerate in the inertial y and z planes. This maneuver causes the missile to climb. Note that the step response will be less than the step command, this is a result of the BTT logic. Also, it should be noted that the acceleration step responses will lose magnitude in steady state, this is due to the fact that the airframe cannot accelerate indefinitely.

TABLE 7. INERTIAL GUIDANCE STEPS
(MACH 2.5, 40,000 FT ALTITUDE)

STEP #	STEPS (g's)	
	a_{y_c}	a_{z_c}
1	25	0
2	0	25
3	25	25
4	25	-25

Figure 19 shows the response to step 1. The solid line in Figure 19 is the achieved acceleration for a_{y_I} and the dashed line is the achieved acceleration for a_{z_I}. From Figure 19, the time response for the step 1 command to 67 percent of the steady state value is approximately 0.5 seconds. This is considerably slower than the baseline autopilot which has a response of 0.3 seconds. The transient response for a_{z_I} is less than that of the baseline autopilot. In Figure 19 there appears to be some instability in the a_{y_I} response at 1.1 seconds. This is not present in the response for the baseline autopilot. The a_{z_I} response shows a bias slightly less than 1. This bias is necessary to offset gravity.

Figure 20 shows the step 2 response. The autopilot achieves 67 percent of steady state at 0.7 seconds. The baseline autopilot achieved steady state at 0.6 seconds. The a_{y_I} transient response in the baseline autopilot is much more severe, with a peak-to-peak magnitude of 8 g's.

Figure 21 shows the step 3 response. The autopilot achieves 67 percent of steady state in 0.6 seconds for both a_{y_I} and a_{z_I}. The baseline acceleration responses were 0.4 seconds and 0.5 seconds respectively. The baseline response has more transients at 1.1 seconds and after 1.4 seconds.

Figure 22 shows the step 4 response. Both inertial accelerations achieve 67 percent of steady state in 0.3 seconds and the baseline autopilot response takes 0.2 seconds. Figures 23, 24, 25, 26, and 27 show α, β, p, q, and r responses for step 4. The response for α is 0.2 seconds less than the baseline α response. There are some other minor differences in the other responses shown and those of the baseline autopilot; however, it appears that the α response difference is the most critical since it is significantly slower than the baseline.

In addition to the steps shown in Table 7, 100 g steps were also used to assess acceleration capability of the missile. Based on these results, the maximum acceleration of the airframe is slightly less than 30 g's.

3. MISSILE-TARGET INTERCEPTS

Three engagement conditions were used to test the autopilot designs. These engagement conditions were used for both the deterministic runs and the Monte Carlo runs. Table 8 shows the missile engagement conditions used, and Table 9 shows the target engagement conditions used.

TABLE 8. MISSILE ENGAGEMENT CONDITIONS

MISSILE		
ENGAGEMENT	ALTITUDE	MACH
1	40,000 ft	2.5
2	40,000 ft	2.5
3	65,000 ft	3.0

TABLE 9. TARGET ENGAGEMENT CONDITIONS

TARGET				
ENGAGEMENT	ALTITUDE	MACH	RANGE	HEADING (degrees off head-on)
1	40,000 ft	2.0	15,000 ft	15
2	40,000 ft	1.1	15,000 ft	180 (Tail Chase)
3	65,000 ft	2.3	15,000 ft	5

4. MONTE CARLO RUNS

Miss distance sensitivity of the autopilot to modeling errors and measurement noise was investigated to determine the effects these have on the miss distances. For the purpose of comparison, the Monte Carlo runs emulated the runs accomplished for the autopilot design of Reference 7. The number of runs per Monte Carlo simulation was 100. Numerous error sources are included in the Monte Carlo simulation. Included in these were sensor noise, sensor scale factor and bias errors, variations on the deviation from the initial conditions, and variations on wind angle and velocity. Also included were variations on the aerodynamic parameters to simulate modeling errors.

In the Monte Carlo simulation the noise sequences used for the measurements are characterized by a normal distribution. At the beginning of each run a random draw was performed to establish the mean and standard deviation for each of the noise sequences used. The random draws themselves are each characterized by a normal distribution, and are established as an input to the simulation.

Tables 10 and 11 contain a brief summary of the Monte Carlo results for engagements 1 and 2. The assumption used in constructing Tables 1 and 2 is that 100 runs per Monte Carlo simulation were enough to treat the miss distances as if they were normal distributions. Only miss distances of 50 feet or less were considered. Performance in engagement 1 is only slightly better than the performance of the baseline autopilot. Performance in engagement 2 is better than the baseline

autopilot performance. Performance of the 65,000 feet, mach 3.0 design in engagement 3 was not compared to the baseline since the Monte Carlo results necessary for a direct comparison were unavailable. In engagement 3, the mean miss distance was 22.3, with a standard deviation of 10.3.

TABLE 10. MONTE CARLO RESULTS FOR ENGAGEMENT 1

MISS DISTANCE SUMMARY	Mean	Standard Deviation
40,000, mach 2.5 design	9.74	8.24
Baseline autopilot	10.40	8.22

TABLE 11. MONTE CARLO RESULTS FOR ENGAGEMENT 2

MISS DISTANCE SUMMARY	Mean	Standard Deviation
40,000, mach 2.5 design	12.10	11.51
Baseline autopilot	16.50	11.63

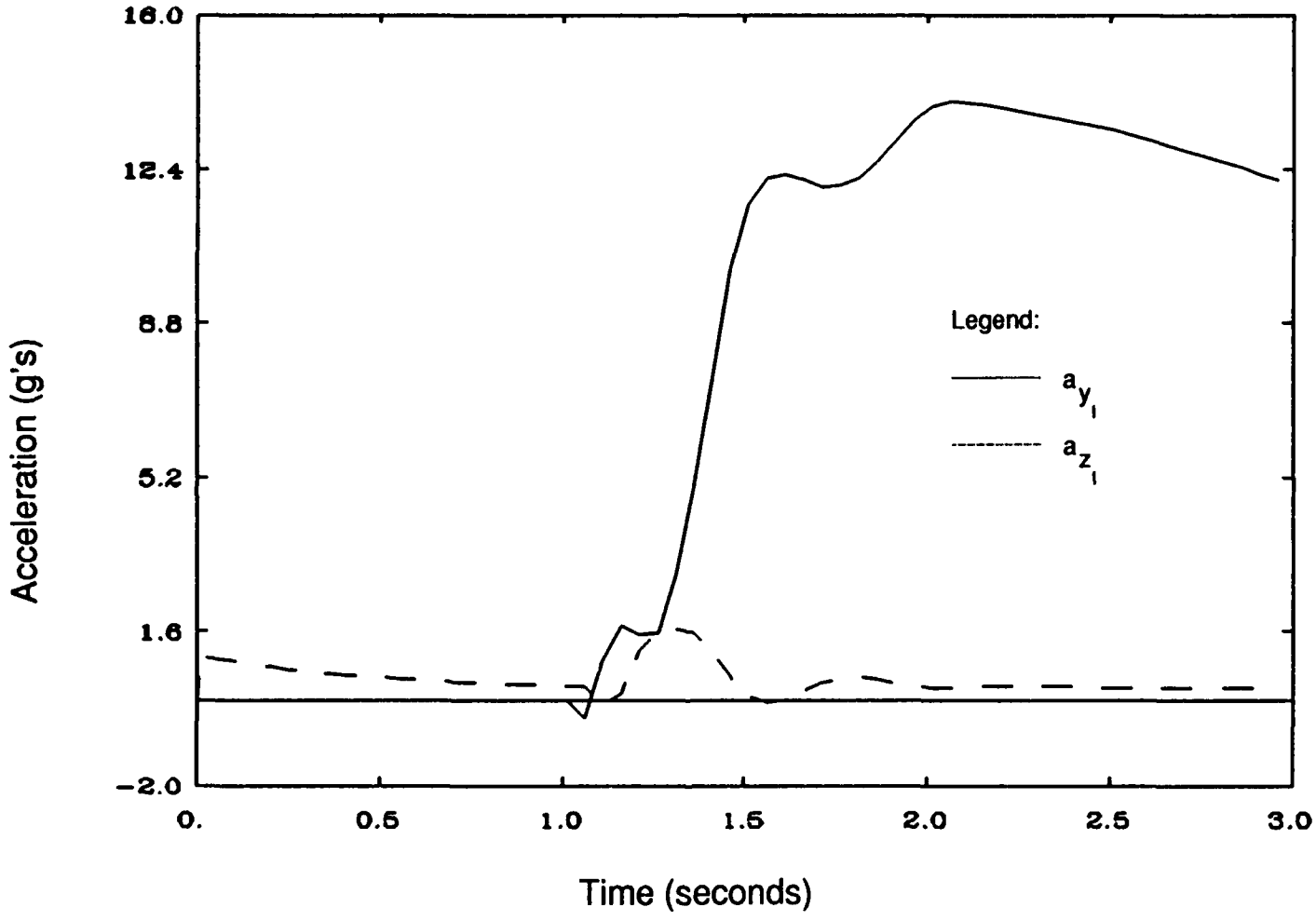

Figure 19. Response for Step 1

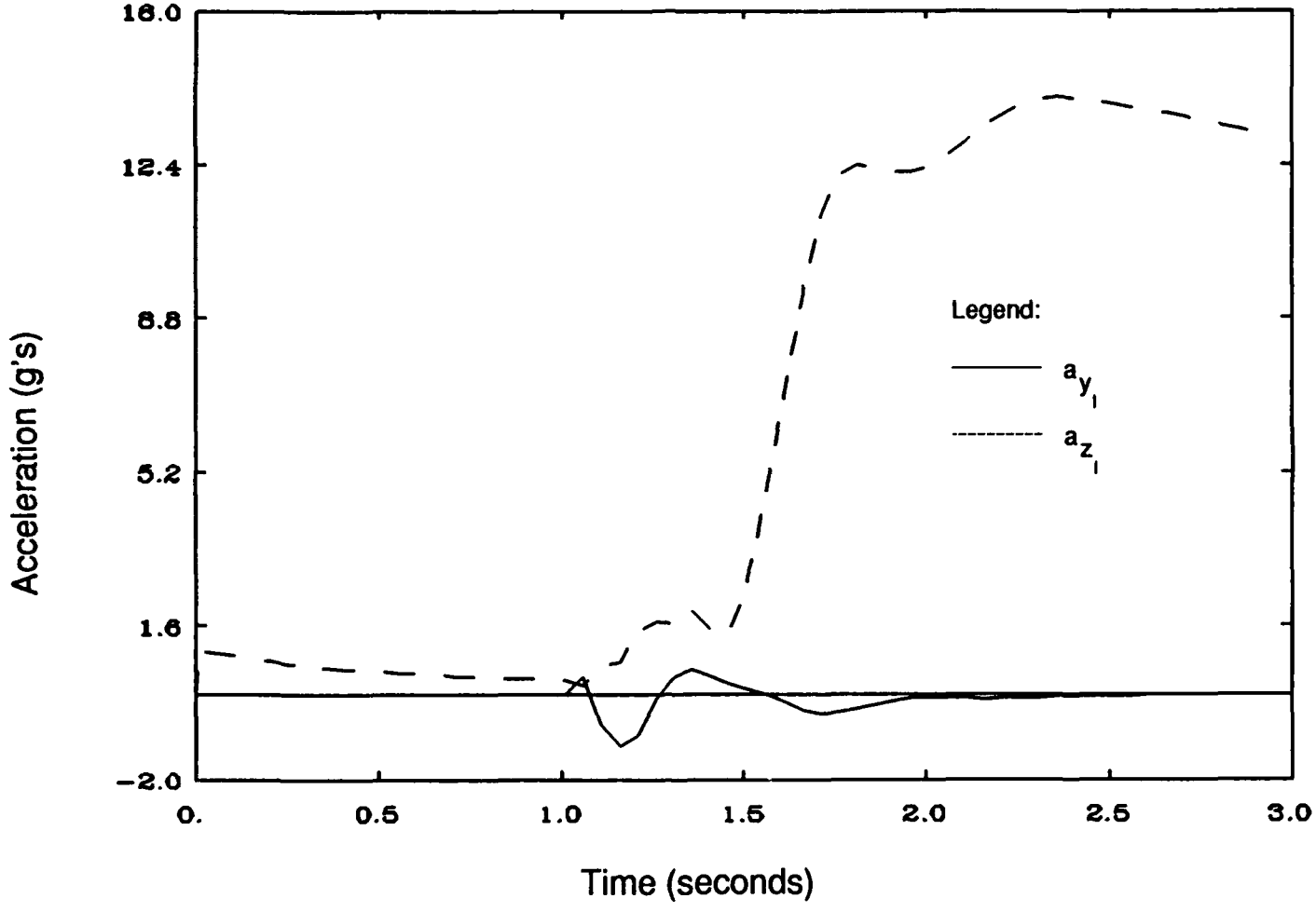

Figure 20. Response for Step 2

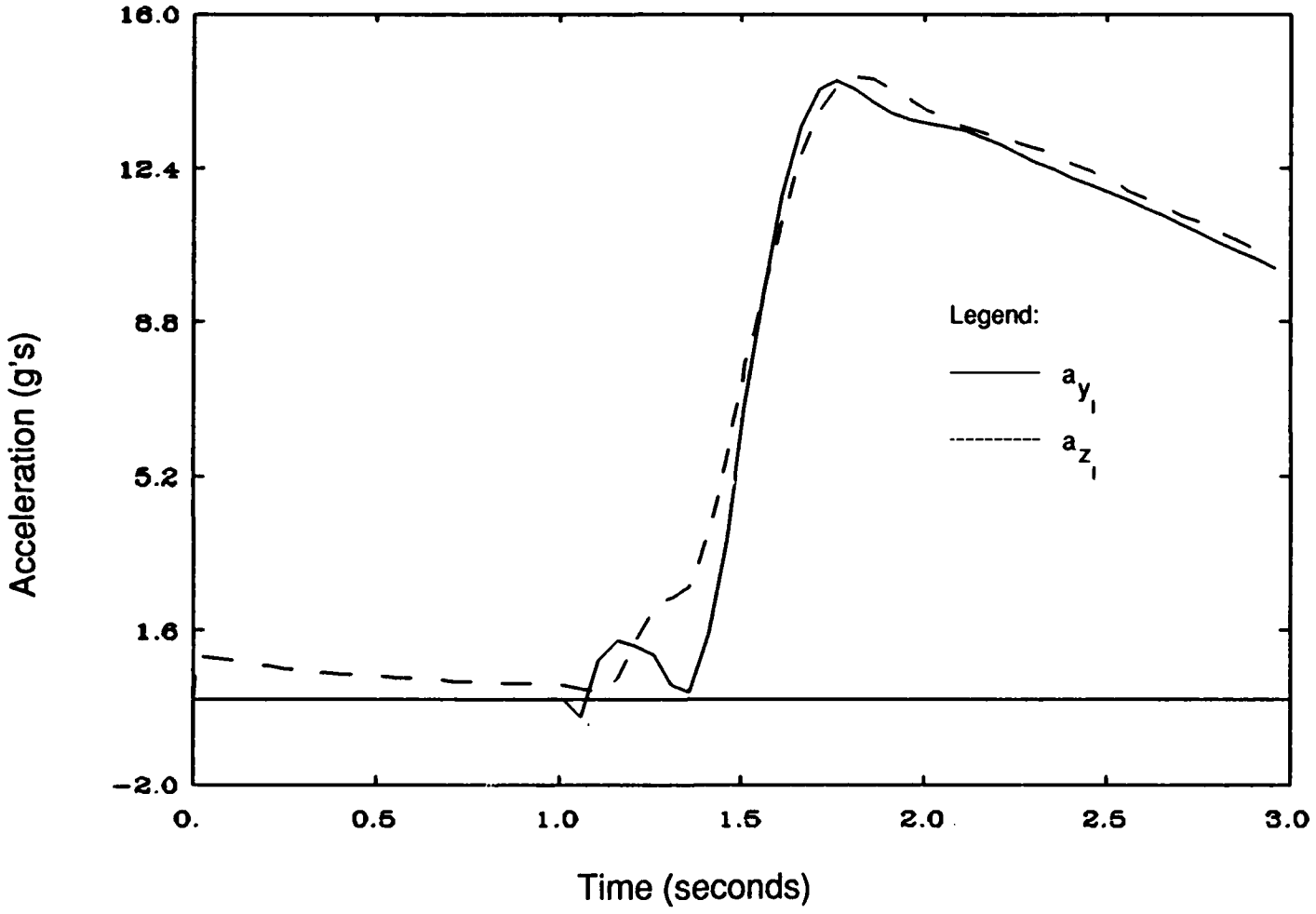

Figure 21. Response for Step 3

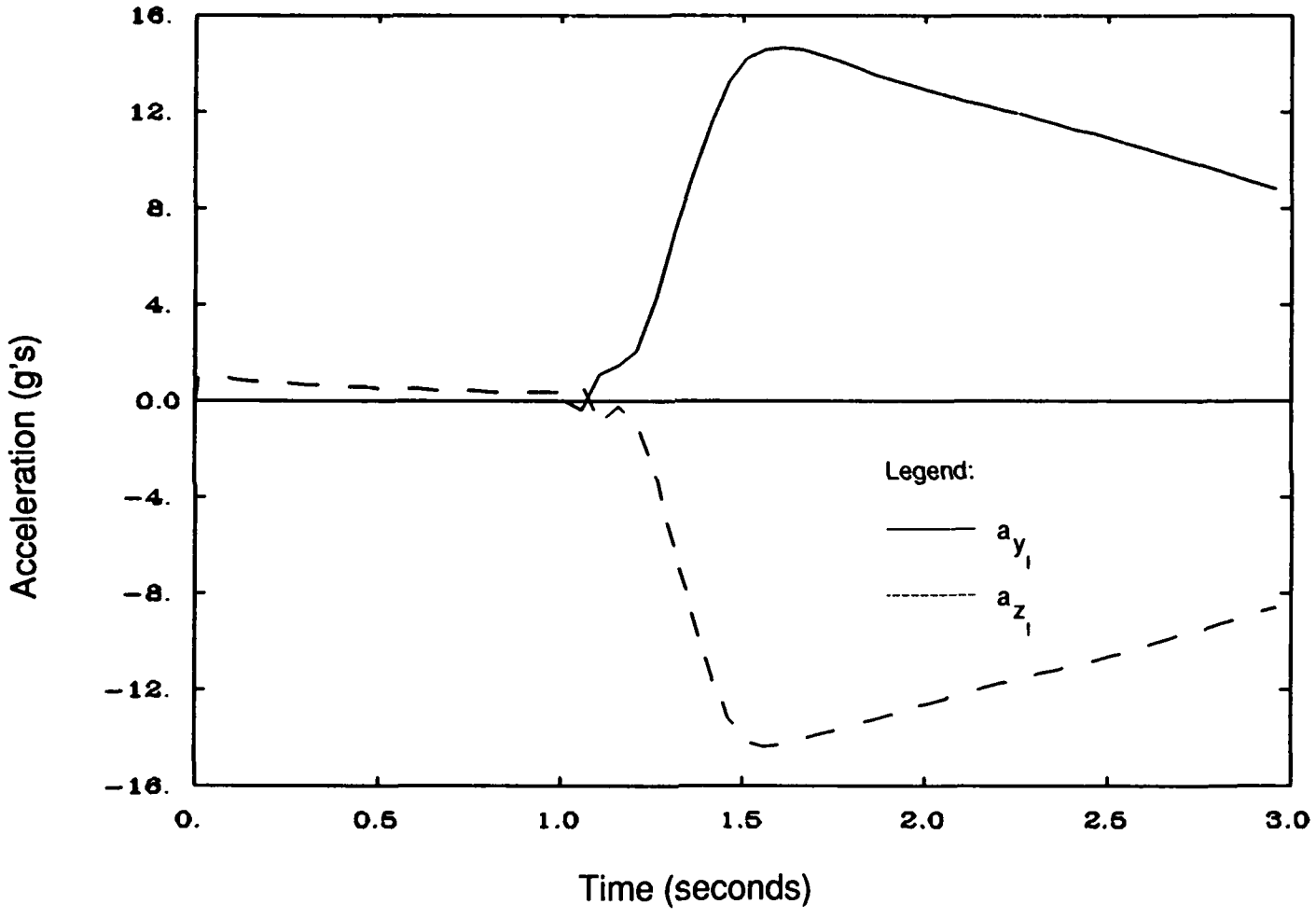

Figure 22. Response for Step 4

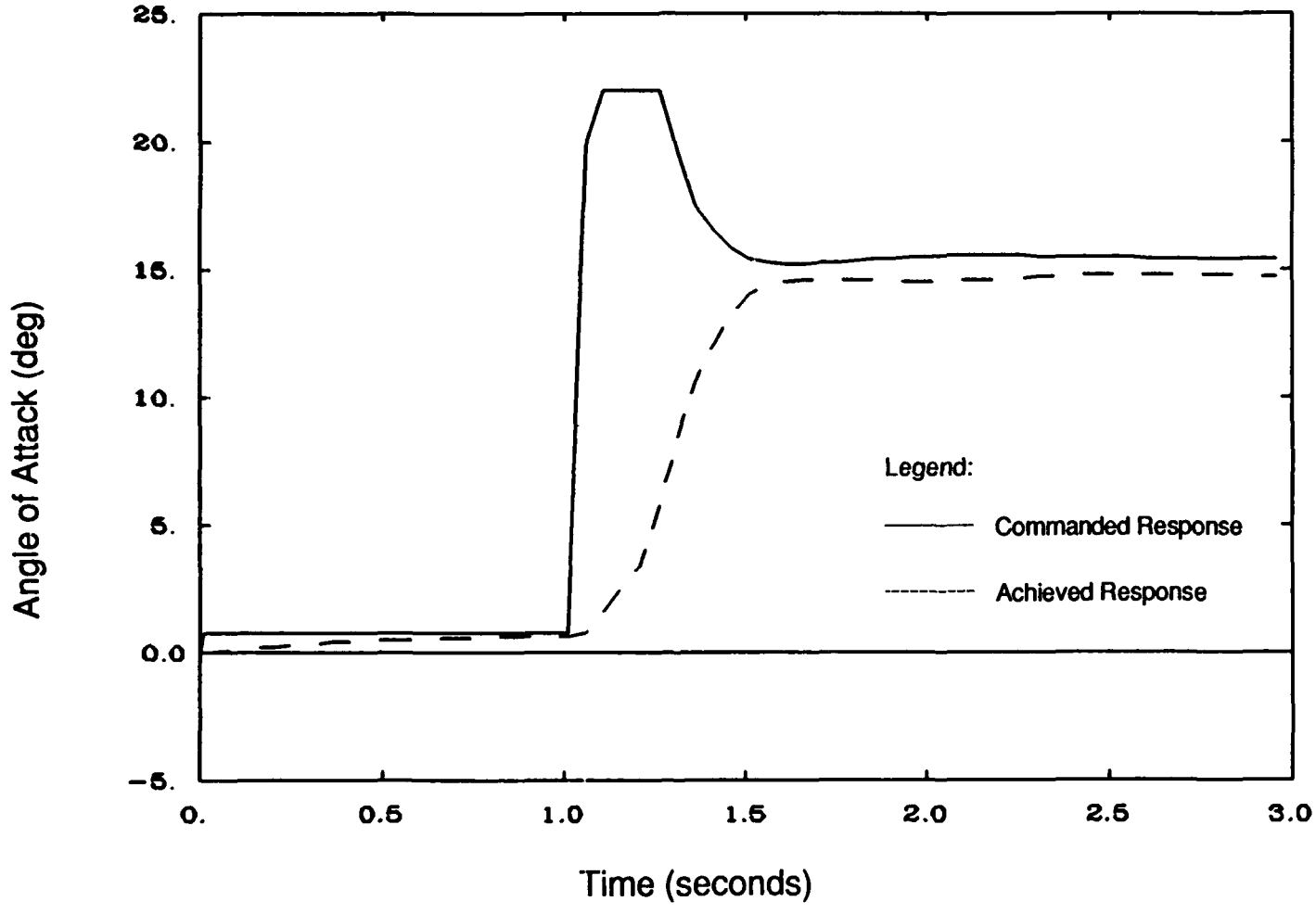

Figure 23. Angle of Attack Response for Step 4

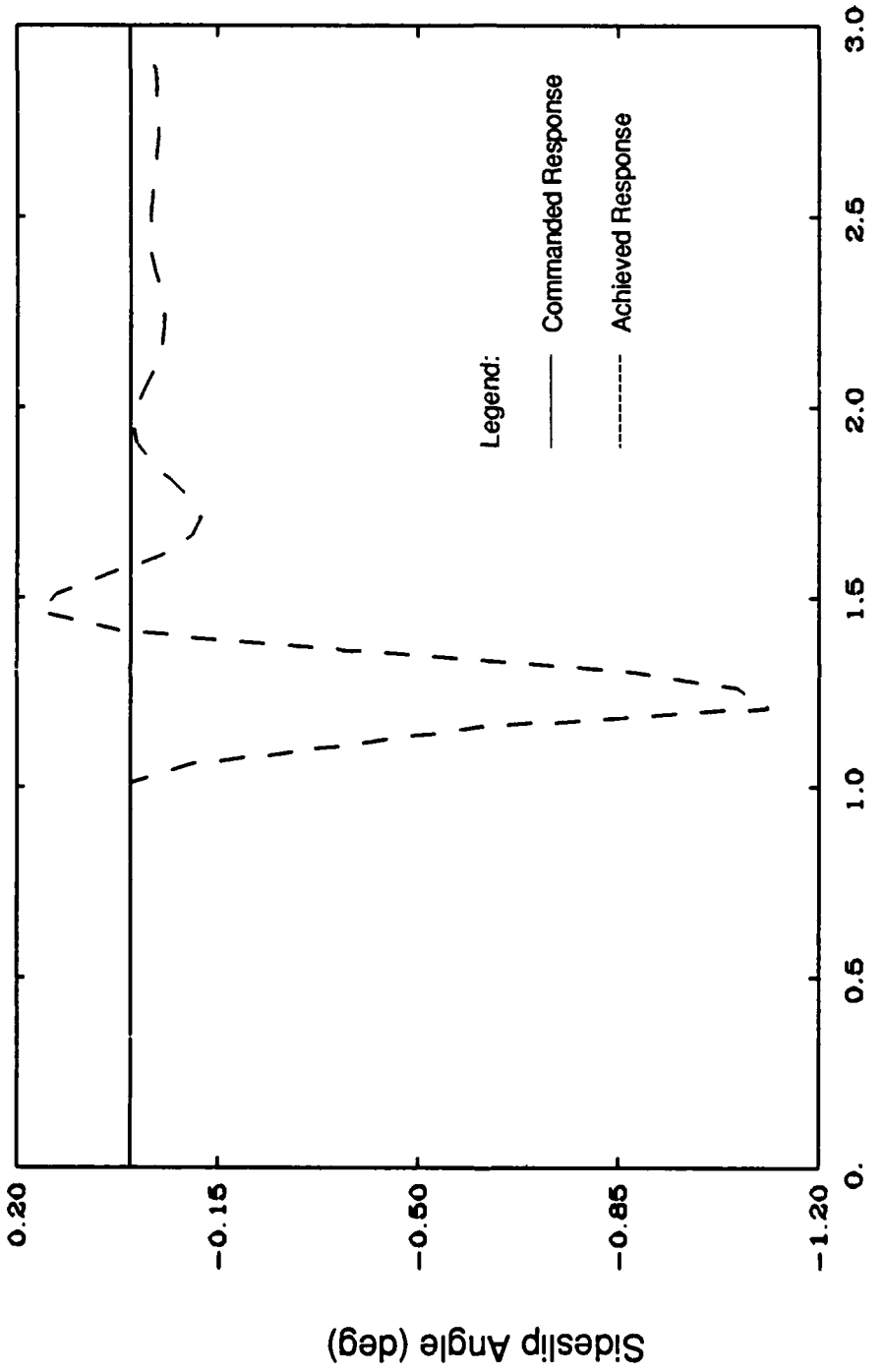

Figure 24. Sideslip Response for Step 4

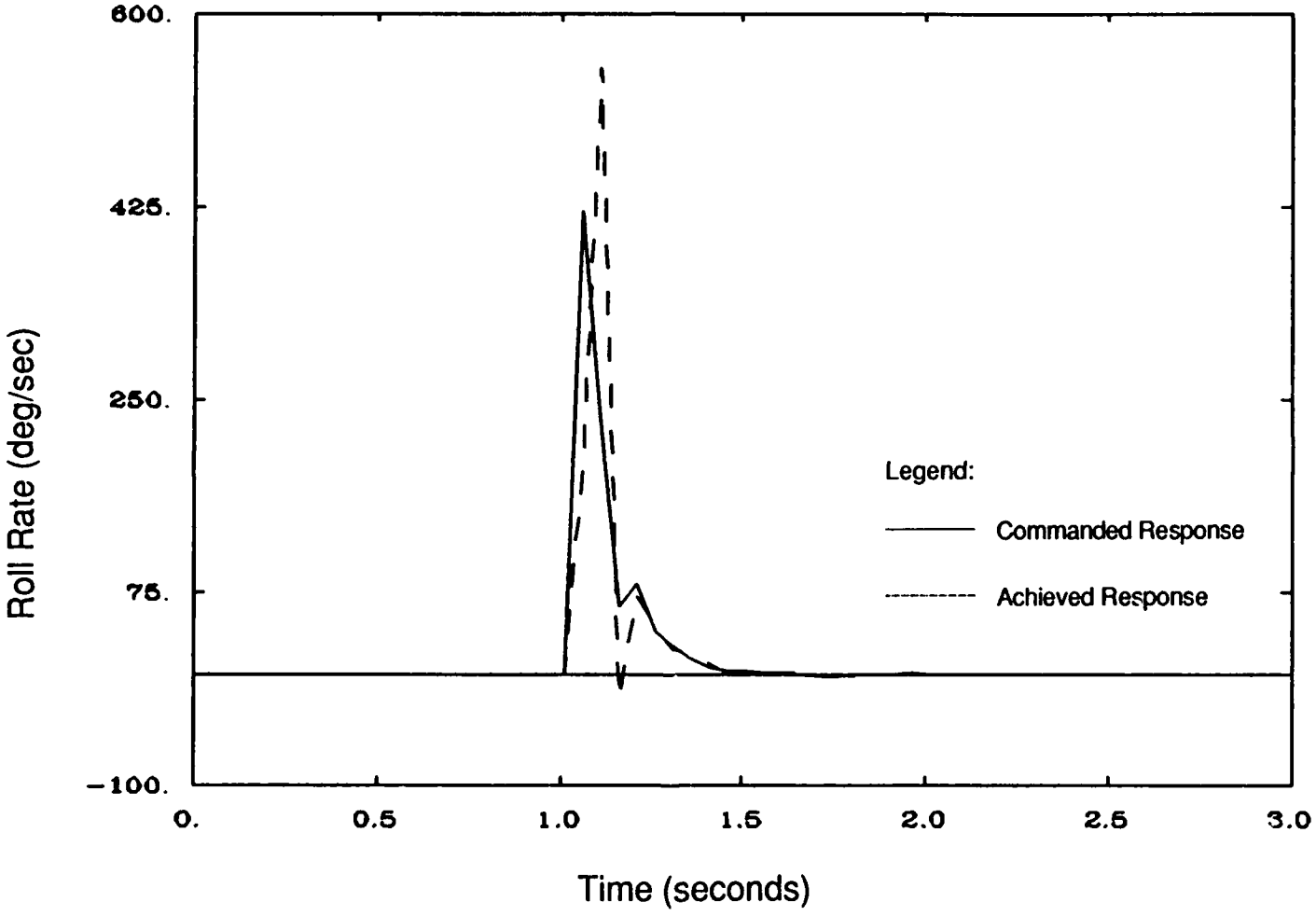

Figure 25. Roll Rate Response for Step 4

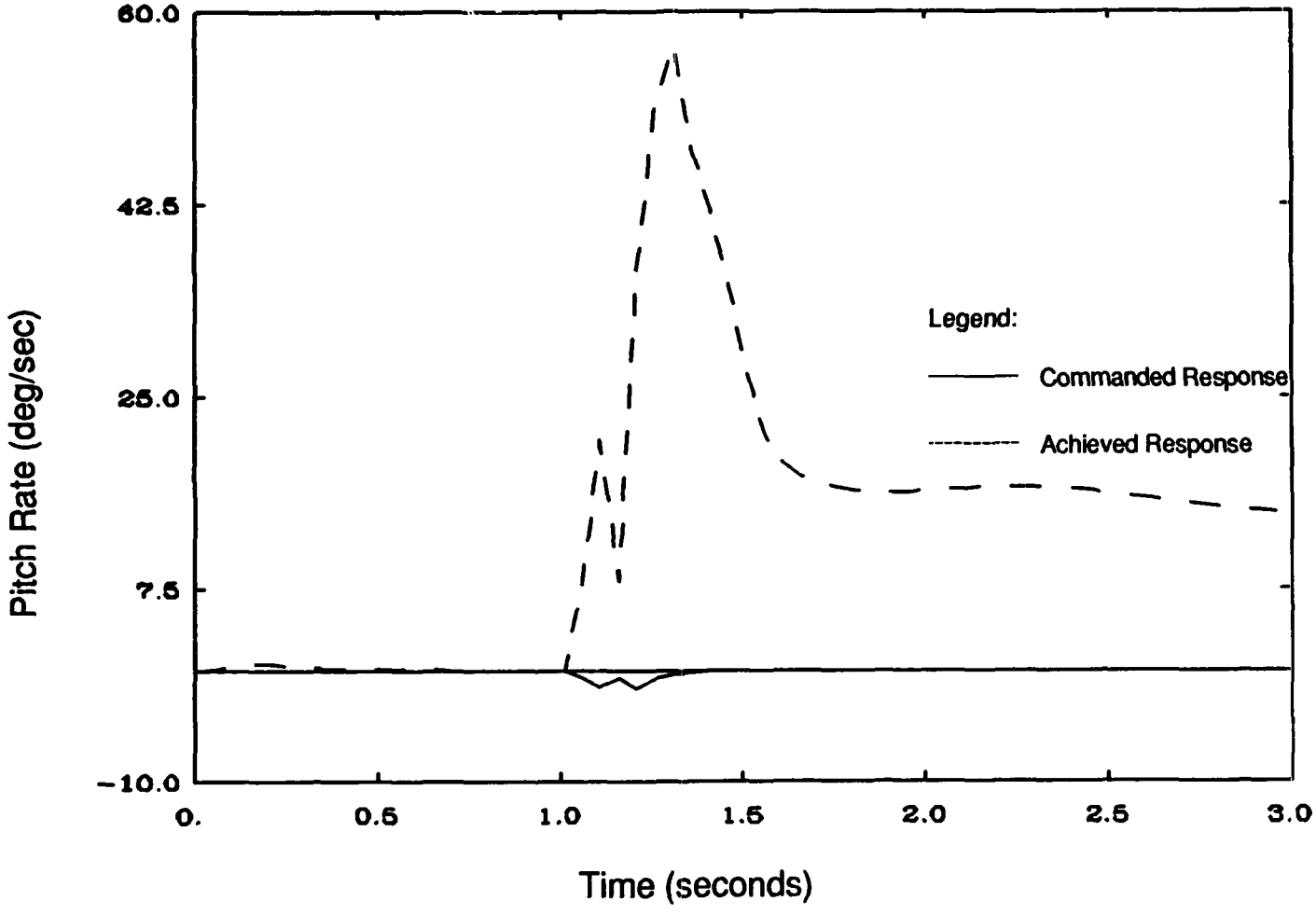

Figure 26. Pitch Rate Response for Step 4

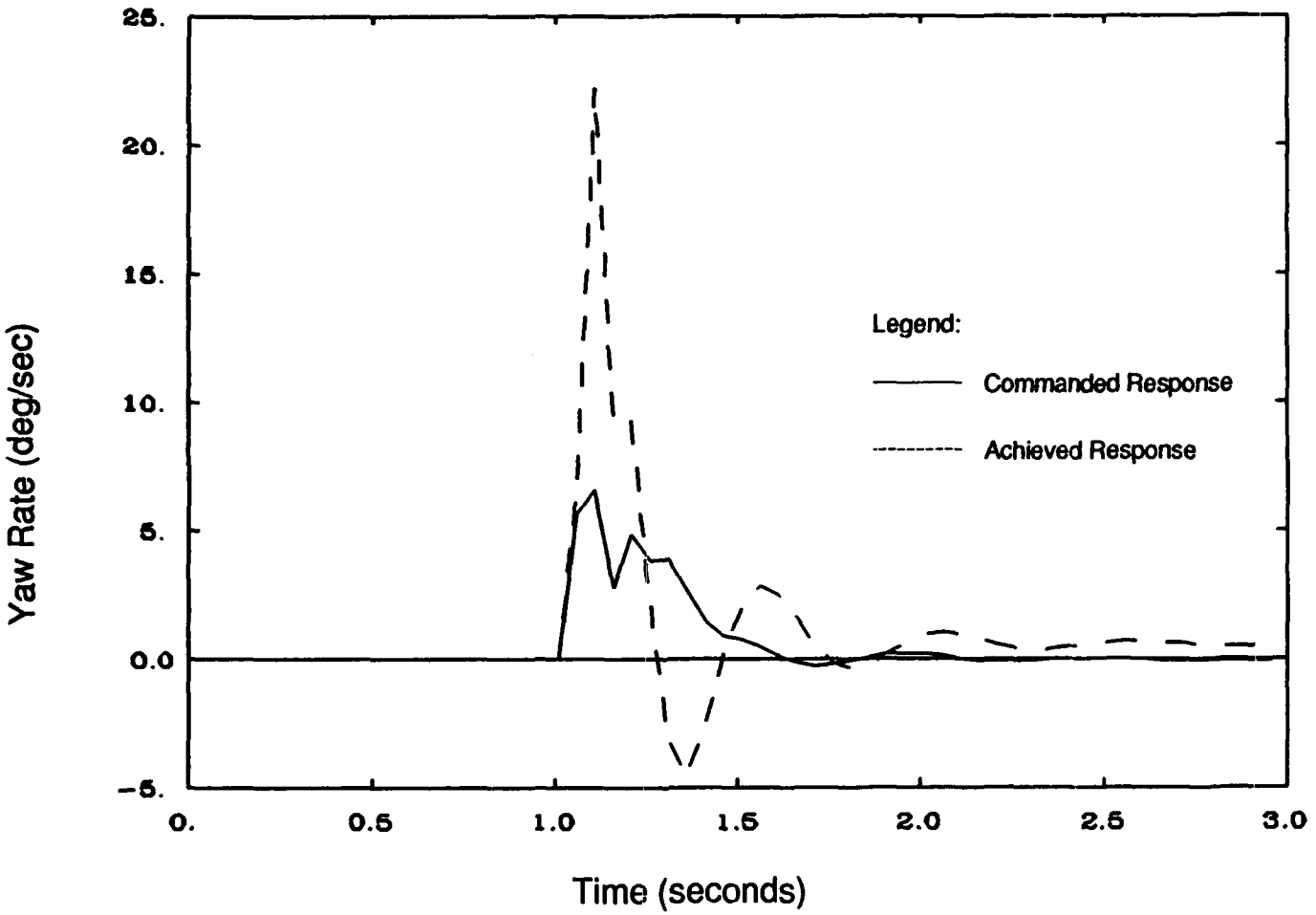

Figure 27. Yaw Rate Response for Step 4

SECTION VIII

CONCLUSIONS AND RECOMMENDATIONS

1. CONCLUSIONS

An autopilot was designed based on the full nonlinear missile dynamics. Performance of the autopilot was evaluated with Monte Carlo simulations. Although deterministic performance of the autopilot is slightly worse than performance of the baseline autopilot, the Monte Carlo simulation of the autopilot demonstrated improved performance over the baseline autopilot. The autopilot response is more damped than the baseline autopilot response. The baseline autopilot leads to more coupling in the acceleration step responses.

The improved Monte Carlo results, and the slower step responses of the autopilot as compared to the baseline autopilot, are due to the tradeoff done for selection of the control weighting matrix (R) used in the regulator design. An improved step response leads to improved deterministic performance, but the autopilot becomes less robust in the presence of sensor noise and more sensitive to modeling errors. For these reasons R was selected to improve the Monte Carlo results.

The approach to the design also demonstrated a way to assess model cross coupling. For the EMRAAT airframe, this approach demonstrated that for decoupled approaches, decoupling the pitch dynamics from the roll and yaw dynamics appears to be good approach. The approach demonstrated the coupling between the roll and yaw dynamics. The approach also demonstrated that some pitch coupling is present in the roll and yaw dynamics. The 65,000 foot, mach 3.0 design, showed only slightly more coriolis and gyroscopic coupling than the designs at 40,000 foot, mach 2.5. In either case, the coriolis and gyroscopic coupling did not pose design or implementation problems.

The stochastic approach used to assess gain scheduling requirements demonstrated that the gain scheduling requirements for the autopilot are minimal and may be scheduled as a function of angle-of-attack and roll rate. Leaving roll rate out of gain scheduling degrades performance, but this is a possible tradeoff if simpler gain schedules are required. The exceptions to this are the gains that vary as a

function of roll rate and couple pitch dynamics into the yaw and roll controls, these gains should not be neglected.

2. RECOMMENDATIONS

a. Model Order Reduction

Based on the results of the approach used in this study, a next generation autopilot design might center around a pitch model and a roll/yaw model. The roll/yaw model would include the coupling from the pitch channel. The advantage to this approach is it results in a reduced set of gains to schedule. This will also allow comparison of this model to the full order model to identify the real benefits of either approach.

b. More Dynamic Flight Envelope

The approach should be extended to a varying flight envelope with larger altitude and mach variations, which leads to larger dynamic pressure variations. A thrusting motor should be included to add the effects of changing missile mass.

c. Reducing Sensitivity to Noise and Missile Flexible Modes

A major drawback of the approach used in this study, was the inability to improve both deterministic performance and performance in the Monte-Carlo simulations. Since the autopilot is working in an environment of noisy measurements and modeling errors, techniques such as LQG/LTR should be employed to reduce sensitivity to noise. Analysis should be extended to include body flexible modes. Notch filters, for example, may be employed to attenuate bending modes.

THE
APPENDIX

EMRAAT AERODYNAMIC DATA

This appendix lists the data used for the extended medium range air-to-air technology (EMRAAT) airframe. The data listed is for the airframe with no fuel (empty weight). The first variables listed are those that do not change.

d Missile Reference Diameter (0.625 ft)

S Missile reference area (0.3067 ft^2)

W Missile Weight (empty) (227 lb)

Moments of Inertia (slug - ft^2):

$I_{XX} = 1.08$
$I_{YY} = 70.13$
$I_{ZZ} = 70.66$

Products of Inertia (slug - ft^2):

$I_{XY} = 0.274$
$I_{XZ} = 0.704$
$I_{YZ} = -0.017$

The following data is a function of the flight conditions. The data is listed for two conditions:

Condition #1:	Angle-of-attack	10 degrees
	Sideslip angle	0 degrees
	Roll rate	0 deg/sec
	Pitch rate	0 deg/sec
	Yaw rate	0 deg/sec
	Altitude	40,000 ft
	Mach	2.5
Condition #2:	Angle-of-attack	10 degrees
	Sideslip angle	0 degrees
	Roll rate	0 deg/sec
	Pitch rate	0 deg/sec
	Yaw rate	0 deg/sec
	Altitude	65,000 ft
	Mach	3.0

Q - Dynamic Pressure (lb/ft^2) :

Condition 1: 1719.93
Condition 2: 749.29

Following are the aerodynamic derivatives (units are per rad). Note that C_{N_α} was obtained by taking the slope of the aerodynamic derivative C_N (not listed).

	Condition 1	Condition 2
C_{N_α}	-50.7067	-47.3550
$C_{N_{\dot{\alpha}}}$	0.0221	0.0182
C_{N_q}	-0.0103	-0.0082
$C_{N_{\delta q}}$	-3.1182	-2.4653

	Condition 1	Condition 2
C_{Y_β}	-16.1902	-16.2871
C_{Y_p}	-0.0004	-0.0003
C_{Y_r}	0.0082	0.0051
$C_{Y_{\delta p}}$	0.2229	0.5171
$C_{Y_{\delta r}}$	3.5252	3.2733

	Condition 1	Condition 2
C_{l_β}	-9.3923	-7.5674
C_{l_p}	-0.0069	-0.0027
C_{l_r}	0.0011	0.0051
$C_{l_{\delta p}}$	-4.0739	-3.2080
$C_{l_{\delta r}}$	-5.5816	-4.7366

	Condition 1	Condition 2
C_{m_α}	-17.6108	-16.8330
$C_{m_{\dot{\alpha}}}$	0.0124	0.0182
C_{m_q}	-0.1329	-0.1043
$C_{m_{\delta q}}$	-25.4394	-20.4340

	Condition 1	Condition 1
C_{n_β}	3.6044	1.9920
C_{n_p}	0.0026	0.0019
C_{n_r}	-0.1231	-0.928
$C_{n_{\delta p}}$	5.8220	5.7507
$C_{n_{\delta r}}$	-28.4375	-25.7876

REFERENCES

1. Arrow, A., "Status and Concerns for Bank-to-Turn Control of Tactical Missiles," Journal of Guidance, Control, and Dynamics, Volume 8, no. 2, March-April 1985, p. 267.

2. Hemsch, M. J., and J. N. Nielsen, Tactical Missile Aerodynamics, Volume 104, "Progress in Astronautics and Aeronautics," Martin Summerfield Series Editor-in-Chief, American Institute of Aeronautics and Astronautics, Inc., Chapter 1.

3. Cloutier, J. R., J. H. Evers, and J. J. Feely,"An assessment of Air-to-Air Missile Guidance and Control Technology," Proceedings of the AIAA American Control Conference, June 1988.

4. Arrow, A., and T. R. Stevens, "Autopilot for Extended Medium Range Air-to-Air Technology Missile," Johns Hopkins Applied Physics Laboratory Report FIE(86)U-1-026, October 1986.

5. Emmert, R.I., and R. D. Ehric. "Strapdown Seeker Guidance for Air-to-surface Tactical Weapons," AFATL-TR-78-60, May 1978.

6. Williams, D. E., B. Friedland, and A. N.Madiwale, "Modern Control Theory Design of Autopilots for Bank-to-turn Missiles," Journal of Guidance, Control, and Dynamics, Volume 10, no. 4, July-August 1987, p. 378.

7. Bossi, J. A., and M. A. Langehough,"Multivariable Autopilot Designs for a Bank-to-turn Missile," presented at the 1988 American Control Conference, Atlanta, June 1988.

8. Arrow, A., and D. E. Williams, "Comparison of Classical and Modern Autopilot Design and Analysis Techniques for a Tactical Air-to-Air Bank-to-Turn Missile," Proceedings of the AIAA GNC Conference, Monterey, Aug 1987.

9. Nesline, F. W., and Zarchan, P. "Why Modern Controllers Can Go Unstable in Practice," Journal of Guidance, Control, and Dynamics, Volume 7, no. 4, July-August 1984, pp. 495-500.

10. Etkin, B., Dynamics of Flight - Stability and Control. New York: John Wiley and Sons, 1982,pp. 107-118.

11. Brogan, W. L., Modern Control Theory, Second Edition. New Jersey: Prentice Hall, 1985, pp. 334-335.

12. Thompson, C. M., E. E. Coleman, and J. D.Blight, "Integral LQG Controller Design for a Fighter Aircraft," AIAA Paper 87-2452-CP, Proceedings of the Guidance, Navigation, and Control Conference, August 1987, p. 866.

13. Franklin, G. F., and J. D. Powell, Digital Control of Dynamic Systems, Addison-Wesley, 1980, Chapter 6 and Appendix A to Chapter 6.